nature portfolio

Peer Review File

Topological Isomerization Unlocks Exceptional Elasticity and Strength of Cellulosic Triboelectric Aerogels

Corresponding Author: Professor Shuangxi Nie

This file contains all reviewer reports in order by version, followed by all author rebuttals in order by version.

Version 0:

Reviewer comments:

Reviewer #1

(Remarks to the Author)
This manuscript presents a topological isomerization strategy to fabricate a cellulosic triboelectric aerogel that exhibits a combination of elasticity, strength, and stable triboelectric output across a wide range of temperatures and humidity. The authors characterize the structural evolution from cellulose I to cellulose III, the construction of a polymer topological network via in-situ interfacial polymerization, and the resulting mechanical and triboelectric performance, supported by molecular dynamics simulations and DFT calculations.
However, the core concept of enhancing hydroxyl accessibility and mechanical properties through competitive hydrogen bonding and crystal transformation, while executed here, bears significant resemblance to previously established strategies in cellulose material science, such as ammonia treatment for cellulose III conversion and silane-based surface functionalization. The mechanism of hydrogen bond disruption and polymer network shielding does not appear to introduce a new principle or paradigm beyond incremental optimization of known approaches. The performance results of the output are not outstandingly superior either. The novelty of this study remains insufficient to meet the high bar for publication in highly esteemed Nature Communications.

Reviewer #2

(Remarks to the Author)
The manuscript introduces a topological isomerization approach that ingeniously reconciles the inherent conflict between strength and elasticity in cellulose aerogels. Beyond its remarkable mechanical attributes, the aerogel also demonstrates consistent triboelectric efficacy, thereby presenting a cutting-edge material solution for self-powered flexible electronics. Overall, this is a meticulous and timely study. I believe it is suitable for publication in Nature Communications, with the following suggestions for improvement:
1. The use of small-molecule ethylenediamine treatment to achieve cellulose crystal transformation in the aerogel state is a key aspect. It is recommended to design a reasonable control experiment to statistically analyze the changes in pore size distribution and pore wall morphology before and after treatment. This would better support the claim that the ethylenediamine treatment does not alter the microstructure of the aerogel.
2. It is noted that ethylenediamine can be recycled and reused during the treatment process. Although this is illustrated in a figure, it should be explicitly mentioned in the main text, as it represents a unique advantage of this manuscript.
3. The authors constructed a polymer topological network in the aerogel via in-situ polymerization, but the manuscript only shows the elemental distribution of C, O, and Si for CNF-III@Si. Including the corresponding data for CNF-I@Si would better demonstrate the beneficial effect of the pretreatment on the in-situ polymerization.
4. It is recommended to supplement the analysis of the pore size distribution of CNF-III@Si aerogels before and after compression to illustrate the structural stability of the aerogel.
5. The molecular structure of CNF-III@Si shown in Figure 3d appears to differ from that in Figure 1a. The currently depicted siloxane linkages between cellulose chains do not fall within the category of polymers and should be appropriately corrected.
6. The topological isomerization strategy enables the CNF-III@Si aerogel to achieve ultra-high elasticity and high strength. The authors provided a detailed analysis of the mechanical performance after 20,000 compression cycles. However, structural changes in aerogels often occur during the initial compression cycles. Therefore, it is recommended that the authors supplement the analysis of the first 500 compression cycles to fully demonstrate the structural stability of the aerogel.
7. To more fully demonstrate the stability of the aerogel's triboelectric performance, it is suggested that the authors

supplement cyclic tests at different temperatures, such as 50 °C, 100 °C and 150 °C, which would better illustrate the superiority of the aerogel's performance.
8. Although CNF-I@Si aerogels do not exhibit mechanical properties as excellent as those of CNF-III@Si, the manuscript lacks a comparison of their triboelectric output performance.
9. Power density is an important reference data for evaluating triboelectric performance. It is recommended that the authors supplement relevant data on power density.
10. The authors claim that the CNF-III@Si triboelectric aerogel exhibits significant environmental tolerance. This should be supported by comparing its performance with other similar aerogels.
11. Another important aspect of triboelectric performance is energy storage capacity. It is suggested to include a comparative analysis of the energy storage capabilities of CNF-I@Si and CNF-III@Si aerogels.

Reviewer #3

(Remarks to the Author)
This work described an interesting topological isomerization strategy in which ethylenediamine treatment induced the transformation of cellulose I to cellulose III, significantly enhancing the hydroxyl accessibility and reactivity of the aerogels. Building on this, an in-situ polymerization approach was used to construct a uniform polymer topological network, enabling the fabrication of cellulose aerogels that combine super elasticity, high mechanical strength, and stable triboelectric output. The material exhibited excellent performance even under extreme temperature and humidity conditions, offering a new paradigm for the development of flexible electronic devices. I recommend acceptance of the manuscript for publication after addressing the following revision comments.
1. This work have thoroughly characterized the microporous structure of the aerogels using SEM, BET, and other techniques, clearly revealing their honeycomb-like morphology and specific surface area features. However, providing additional insight into how the topological isomerization influences pore orientation or nanoscale ordering would further enhance the rigor of the manuscript.
2. It stated that silanization enhances thermal stability, but it lacks an analysis of how the Si–O covalent network contributes to the thermal decomposition behavior. It is recommended that the authors further interpret the protective effect of the Si–O network based on the TGA/DTG results.
3. The discussion of hydrogen-bond network relaxation in CNF-III was primarily supported by molecular dynamics–derived hydrogen-bond statistics (Figure 2c) and deconvolution of FTIR hydroxyl peaks (Figure 2d–e), which provided only indirect evidence of hydrogen-bond weakening. Direct experimental characterization of hydrogen-bond energy changes or conformational transitions would more convincingly support the core mechanistic pathway of “hydrogen-bond weakening → chain relaxation → altered thermal decomposition behavior.”
4. To strengthen the reliability of the conclusions related to the material’s “super elasticity” or “structural robustness,” it is recommended that the authors include microstructural characterization after cyclic compression.
5. The current manuscript reported thermal conductivity only in a single direction; however, for cellulose-based aerogels or other porous materials, pore alignment, fiber orientation, and the distribution of the surface silanization layer may led to pronounced anisotropy in thermal conductivity. Presenting data from only one direction may not fully reflect the material’s actual heat-transfer capability and makes it difficult to determine whether the topological isomerization or silanization processes alter the heat-flow pathways within the microstructure network.
6. It stated that CNF-III underwent more extensive silanization due to its higher hydroxyl accessibility. However, this conclusion was currently based mainly on XPS survey elemental ratios (Figure 3f) and FTIR spectra (Figure S8a) and may still lack direct experimental evidence capable of quantifying the actual reaction extent. It is recommended that the authors provide characterization methods that can quantify the Si content or the degree of silanization.
7. This work evaluated the triboelectric performance mainly through macroscopic output parameters such as open-circuit voltage and short-circuit current. It is recommended that the authors further quantify the surface charge density to more accurately assess how topological isomerization or silanization influences the triboelectric charging behavior of the material.

Reviewer #4

(Remarks to the Author)
The manuscript presents several noteworthy results. It demonstrates the conversion of cellulose I to cellulose III within a preformed aerogel architecture, enabling a subsequent vapor-phase siloxane crosslinking that produces an aerogel with exceptionally high elasticity, mechanical resilience, and stable triboelectric output. The combination of allomorph engineering, surface reactivity enhancement, and triboelectric performance is clearly interesting for areas including cellulose materials science, aerogel design, flexible electronics, and sensor development.
Overall, the data support the main conclusions, and many of the mechanical and triboelectric results are convincing. However, several aspects require clarification or deeper explanation—for example, the interpretation of hydrogen-bond distributions, the thermal degradation behavior of CNF-III, and the relationship between MD/DFT analyses and the experimental findings. These points do not invalidate the study but require revision to ensure the conclusions are fully supported.
The work has potential significance because it combines cellulose chemistry with a siloxane topological network to overcome the classical trade-off between strength and elasticity in CNF aerogels. The reported performance exceeds many literature benchmarks. At the same time, the conversion of cellulose I to cellulose III via amine treatment is well-established, so claims of conceptual novelty or “topological isomerization” should be contextualized more carefully within the existing literature.
The experimental approach is generally sound and appropriate for the study’s aims. However, several methodological

descriptions lack detail for ease in reproducibility—particularly the EDA treatment and washing protocol, the MTMS vapor-phase deposition setup, triboelectric testing parameters, and aspects of the MD workflow. More details will strengthen the manuscript. I am not an expert in MD or DFT simulations, but I note that the descriptions of these methods should be made fully consistent with the detailed procedures given in the Supplementary Information.
The analytical framework is mostly appropriate, but several interpretations require further justification—especially reconciling FTIR hydrogen-bond assignments with MD results, explaining early thermal degradation of CNF-III aerogels, and addressing limitations of the DFT model systems. These refinements will improve the robustness of the conclusions.
The manuscript would be strengthened by clearer methodological descriptions, additional explanations for specific contradictory or unclear findings, and more cautious framing of novelty claims. These revisions are well within the scope of a typical resubmission and do not require fundamentally new experiments.
The manuscript is generally well written and accessible. Some sections, however, would benefit from additional contextualization—e.g., the introduction includes results and the discussion is very minimal.
The manuscript cites relevant literature but should also acknowledge prior foundational work on amine-induced cellulose III formation and established cellulose surface-reactivity concepts.
This review was prepared together with the Early Carrer Researcher Jeannie Egan following the co-review initiative. We are not experts in molecular dynamics or DFT, and our comments in these areas focus on clarity and consistency rather than technical depth.
The comments and further additions are listed in detail below:
Line 76: “CNF-III@Si” appears for the first time and should be defined in its first instance in the paper.
Line 88: Paradigm feels too strong here.
Line 105: The Cell III allomorph is formed during EDA treatment, not after. This is presented misleading. Enter a “has”: … the crystal from has transitioned. Further, “guest” feels like a weird word. Better use something like “tempoararily bonded”.
Line 124: “topoisomerization”. We suggest to keep the language consistent: topological isomerization.
Figure 1d: there are several misspellings in the image: Carbon mocrolattices --> microlattices; Cubic raphene aerogels --> cubic graphene aerogels; Elastic but week --> elastic but weak; Yong’s modulus --> Young’s modulus
Figure 1e: also a small misspelling: TEGN --> TENG (for triboelectric nanogenerator)
Line 145: The O2-O6, O3-O6 hydrogen bonds are intramolecular bonds that stiffen the cellulose chain and the O3-O5 hydrogen bond is intermolecular between the cellulose chains. The authors may want to work that out in the text to the reader for a better understanding why the O2-O6 reduces stiffness.
e.g. Credou, J. and T. Berthelot, Cellulose: from biocompatible to bioactive material. Journal of Materials Chemistry B, 2014. 2(30): p. 4767-4788.
This sounds understandable and expectable to me, but on the other hand you write:
Line 179: Figure 2d and Table S3 report an increase of O2-O6 hydrogen bonds from 7.5 to 10.6% and a reduction of the other two in an approximate ratio of 2:1 (B:C). Please provide an explanation for this finding and how it fits with the simulation data.
Line 176: Figure 5 shows that below 150°C there is a lot of crystal water in Cell-I and much more in Cell-III. Thermal degradation in Cell-III seems to start before 200°C. Please explain. Is that because of remaining residues, e.g. of ethanolamine? Ammonia may cause autocatalytic degradation.
Since the thermal conductivity experiments were performed at 200°C. How do these results fit together? TGA of Silica-containing gels are not presented. Please explain. Discuss if the washing process was sufficient to remove the solvent and if incomplete removal contributes to the observed TGA effect.
Line 191: I recommend adding “at the surface”: “…possess a greater number of active hydroxyl groups at the surface and…”
Line 262: “…. Minimal plastic deformation.” I agree that the properties are superior to the comparative materials, however I can recognize a reduction of about 40% in Fig. 4d. Is that correct?
Line 317: Delete “characteristic”.
Line 327: The output signal changed less than 0.5% correct?. If yes, remove “rate”.

The description of materials and methods is sometimes vague and lacks details:
Line 366 ff: Did the volume change after freeze drying. If yes, how much? Were the gels stored in the desiccator afterwards?
Line 373 ff: How often was the rinsing process performed. How did you decide on the rinsing process? This is relevant in view of potential incomplete removal of the solvent.
Line 379 ff: Please provide the reactor volume and if the reactor was purged with an inert gas. Did you use deionized water?
Line 392: Was TGA performed in air or nitrogen? I suppose nitrogen atmosphere since in S5 you write pyrolysis.
Line 411ff: More details needed. Voltage, cycles per second (2 per second?).

Supplement:
Supplementary Note 2: Molecular Dynamics Simulation details:
Last section, torsion angles: check the order of the mentioned tables. Should it be Tables S1 and S2 instead of Tables S3 and S4, as mentioned in the manuscript line 155?
Figure S9: The caption is not correct. There should be a and b instead of c and d.
Figure S11 is lacking the “S”.

Additionally, I would like to mention:
The paper introduces this as a new concept, but the underlying chemistry (Cellulose I → Cellulose III via amines) is well-known. Please contrast the definition with traditional cellulose polymorph conversion. Clarify what is topological beyond crystallographic rearrangement and remove novelty overstatements.
DFT is performed on monomeric fragments of CNF-III@Si, which may not accurately capture the continuum Si–O–Si network. Authors should discuss limitations.

Reviewer #5

(Remarks to the Author)
I co-reviewed this manuscript with one of the reviewers who provided the listed reports. This is part of the Nature Communications initiative to facilitate training in peer review and to provide appropriate recognition for Early Career Researchers who co-review manuscripts.

Version 1:

Reviewer comments:

Reviewer #2

(Remarks to the Author)
The current manuscript has perfectly addressed my questions and is ready for publication in Nature Communications.

Reviewer #3

(Remarks to the Author)
In this revised paper, authors revised the paper according to the comments. Therefore, it can be accepted now.

Reviewer #4

(Remarks to the Author)
I thank the authors for the thorough, careful, and technically detailed revision of the manuscript. The revised version addresses all major and minor comments raised in the initial review in a comprehensive and convincing manner. The authors have significantly improved the clarity and rigor of the manuscript.
One minor point remains regarding the manuscript structure. In the initial review, I suggested strengthening the Discussion section. While the authors have added a clarifying sentence, the standalone Discussion remains relatively short, whereas the Results section is very extensive and already contains a substantial amount of interpretation and contextual discussion. To better reflect the actual content and improve readability, I recommend renaming the Results section to “Results and Discussion”, and renaming the current Discussion section to “Conclusion” if the journal allows this. This is an editorial adjustment and does not require additional experimental or analytical work.
Overall, the manuscript has been significantly strengthened and now meets the standards of scientific clarity, methodological rigor, and internal consistency expected for publication. I recommend acceptance of the manuscript.

Reviewer #5

(Remarks to the Author)
I co-reviewed this manuscript with one of the reviewers who provided the listed reports. This is part of the Nature Communications initiative to facilitate training in peer review and to provide appropriate recognition for Early Career Researchers who co-review manuscripts.

Point-by-Point Response to Reviewers' Comments

We would like to thank you and the reviewers for the thoughtful and constructive comments on our manuscript entitled "*Topological Isomerization Unlocks Exceptional Elasticity and Strength of Cellulosic Triboelectric Aerogels*" (Manuscript ID: NCOMMS-25-87076). These comments are valuable and very helpful in improving our paper. We have tried our best to study all comments carefully and revise the manuscript according to the constructive comments and suggestions.

Our responses are marked in blue, and the revised portions are marked in red. As follows:

Reviewer #1 (Remarks to the Author):

This manuscript presents a topological isomerization strategy to fabricate a cellulosic triboelectric aerogel that exhibits a combination of elasticity, strength, and stable triboelectric output across a wide range of temperatures and humidity. The authors characterize the structural evolution from cellulose I to cellulose III, the construction of a polymer topological network via in-situ interfacial polymerization, and the resulting mechanical and triboelectric performance, supported by molecular dynamics simulations and DFT calculations.

Response: We sincerely thank the reviewer for the comprehensive evaluation and insightful summary of our manuscript. We are pleased that the reviewer recognizes the systematic nature of this work, particularly in terms of structural evolution, topological

network construction, and the correlated analysis of mechanical and triboelectric properties, as well as the supporting roles of molecular dynamics simulations and DFT calculations. We fully appreciate the reviewer's high standards, and it is precisely in light of these standards that, in the revision, we seek to further clarify the core conceptual innovations of this work and articulate its fundamental distinctions from existing studies.

However, the core concept of enhancing hydroxyl accessibility and mechanical properties through competitive hydrogen bonding and crystal transformation, while executed here, bears significant resemblance to previously established strategies in cellulose material science, such as ammonia treatment for cellulose III conversion and silane-based surface functionalization. The mechanism of hydrogen bond disruption and polymer network shielding does not appear to introduce a new principle or paradigm beyond incremental optimization of known approaches. The performance results of the output are not outstandingly superior either. The novelty of this study remains insufficient to meet the high bar for publication in highly esteemed Nature Communications.

Response: We thank the reviewer for the rigorous examination of the originality of this study and for the constructive criticism provided. We fully understand and respect this high standard, and have taken this opportunity to carry out a systematic revision of the manuscript. In particular, we have strengthened the distinctiveness and scientific substance of this work relative to existing cellulose modification strategies, with a focus on clearer conceptual definition, deeper mechanistic elucidation, and more rigorous

performance evaluation. Accordingly, we address the reviewer's concerns from three perspectives: (i) the significant similarity to established strategies, (ii) whether a genuinely new principle or paradigm is introduced, and (iii) the output performance. The detailed responses are provided below：

(i) Clarification regarding the "significant similarity to established strategies"

In response to your concern that the core concept of this work shows significant similarity to previously established strategies, we respectfully provide clarification from the following aspects: ① the overall objective of this study; ② the relationship between competitive hydrogen bonding and crystal transformation and prior studies; and ③ the distinctions between the silane-based surface functionalization employed here and existing approaches. The detailed discussion is presented below.

① Overall objective of this study

A major challenge faced by cellulosic triboelectric aerogels in practical applications is their insufficient elasticity and mechanical strength, which severely compromises the stability of triboelectric output and thus limits their real-world applicability. In this work, a topological isomerization strategy is proposed to resolve the long-standing trade-off between elasticity and strength, while simultaneously achieving stable output under high-humidity and high-temperature conditions. Therefore, the overall research objective of this study is fundamentally different from that of previous works. Accordingly, we have revised the manuscript to more clearly articulate the research objectives and the scientific essence of the proposed innovation, as detailed below:

Revision: … Topological isomerization, which induces electron cloud redistribution

and alters microstructure, enhances triboelectric output performance. Consequently, triboelectric nanogenerators constructed from aerogels exhibit rapid response times and highly stable outputs. Moreover, the stable output signal, sustained across a broad range of temperatures and humidity levels, underscores its significant potential for high-precision flexible sensing in extreme environments. The molecular chain topological isomerization strategy elucidated in this study offers innovative approaches for addressing the elastic design of bio-based materials, as well as a broader spectrum of brittle porous materials, thereby significantly advancing the development of next-generation sustainable flexible electronic devices. (Manuscript, page 5, lines 91-101)

② Relationship between competitive hydrogen bonding and crystal transformation and prior studies

We agree with the reviewer's observation that the competitive hydrogen bonding and crystal transformation involved in this work bear superficial similarities to established approaches in the cellulose materials field. To address this concern, we have clarified the distinctions between our study and conventional amine treatments. In traditional amine treatment of cellulose, competitive hydrogen bonding between cellulose and ethylenediamine induces the transformation from cellulose I to cellulose III, a mechanism that has been well established and that we fully acknowledge.

In contrast to conventional cellulose amine treatments, the amines used in this study are applied to cellulosic aerogels, which are pre-formed structural materials. By leveraging this established mechanism, we enable increased surface exposure of hydroxyl groups while preserving the integrity of the macroscopic porous architecture. In addition,

through a combined experimental and molecular dynamics simulation study (Fig. R1), we further investigate the influence of crystal transformation on the hydrogen-bonding network in greater depth. Our contribution therefore lies in extending and deepening the application of this mechanism specifically to cellulosic aerogel systems.

The original manuscript may not have sufficiently emphasized this relationship; accordingly, we have revised the explanation of competitive hydrogen bonding and crystal transformation as follows:

To highlight the distinctions from conventional amine treatment, we have made the following revisions:

Revision: … The application of amines in the treatment of cellulose has been demonstrated to enhance its reactivity by increasing the exposure of active hydroxyl groups and reconstructing hydrogen bond networks[13–15]. For instance, amine treatment can facilitate isomerization, converting cellulose I into cellulose III, which increases the number of hydrogen bonds in the cellulose chains that are accessible to the aqueous solvent[16]. This transformation significantly improves the binding affinity of cellulose to enzymes. Although cellulose III exhibits heightened sensitivity to specific chemical treatments, there are limited reports on the further functionalization of cellulose aerogels or amine-treated fibers[17,18]. (Manuscript, page 3, lines 47-55)

To more clearly illustrate the structural effects induced by the ethylenediamine treatment, we have made the following revisions:

Revision: … During EDA treatment, the crystal form transitions from cellulose I to cellulose III (CNF-III), which is retained after removal of the temporarily bonded EDA

(Fig. 1a). The EDA employed in this process can be recovered and reused via vacuum distillation, achieving a recovery rate of approximately 90%. Variations in N_2 adsorption and pore distribution indicate that the pore size of the micropores or mesopores remained largely unchanged (Supplementary Fig. 1 and 2). Additionally, SEM images reveal that the pore walls and structure were intact before and after ethylenediamine treatment (Supplementary Fig. 3). These pieces of evidence suggest that the treatment of CNF-I aerogel with EDA does not modify its three-dimensional pore architecture and maintains its original honeycomb porous structure. (Manuscript, page 6, lines 116-126)

To more clearly clarify the purpose of the amine treatment, we have made the following revisions:

Revision: … The conversion of cellulose I to cellulose III through amine treatment is a well-established process. Previous studies have demonstrated that cellulose III is typically more reactive than both cellulose I and cellulose II in the preparation of cellulose derivatives[24,25]. In this study, the crystal isomerization induced by ethylenediamine treatment of CNF-I aimed to expose a greater number of active hydroxyl groups on the fiber surface, thereby facilitating chemical modification. (Manuscript, page 8-9, lines 156-161)

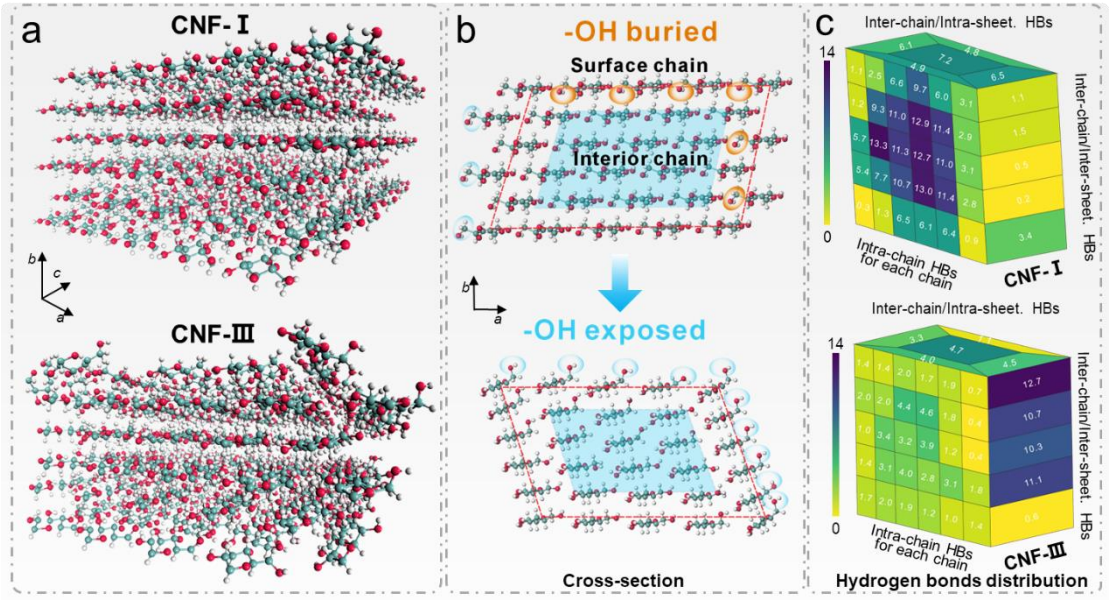

Figure R1. Cellulose crystal isomerization enhances hydroxyl accessibility. (**a**) Unit cell structures of CNF-I and CNF-III. (**b**) Cross-section of the unit cell. (**c**) Distribution of hydrogen bonds within the crystal (see Supplementary Fig. 4 for more details).

③ Distinctions between silane-based surface functionalization and existing studies

We thank the reviewer for pointing out the potential similarities between this work and previously reported silane-based surface functionalization strategies. From an apparent outcome perspective, both approaches involve introducing polymeric or organic networks into cellulose systems to improve mechanical properties and functional stability, which may understandably lead to a perception of similarity. We therefore wish to further clarify the distinctions.

In this study, a continuous polymeric topological network is constructed *in situ* via interfacial polymerization on and within the highly reactive surfaces of the cellulosic aerogel (Fig. R2). This network effectively suppresses irreversible fiber–fiber adhesion during compression (Fig. R3), while preserving the intrinsic stiffness and load-bearing

capability of individual cellulose fibers. It is precisely this structure regulation dominated by topological polymer network constraints that enables the simultaneous realization of high strength and ultrahigh elastic recoverability within a single material system. At the structural level, this approach overcomes the commonly encountered elasticity–strength trade-off in cellulosic aerogels and further ensures stable triboelectric output.

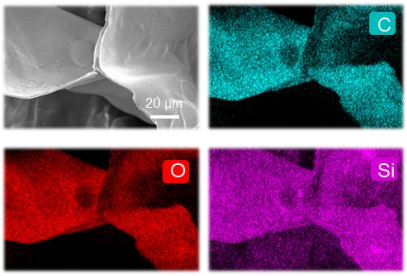

Figure R2. SEM image and EDS elemental distribution of the pore wall of CNF-III@Si aerogel.

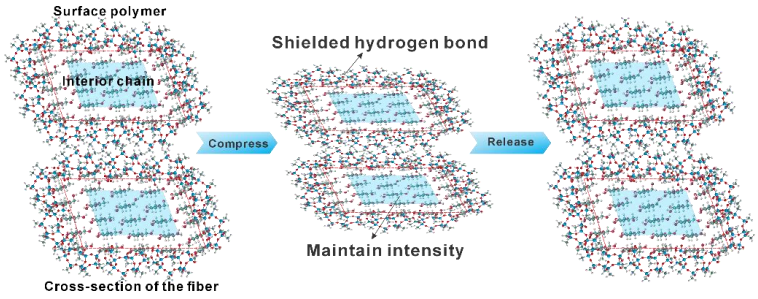

Figure R3. CNF-III@Si fibers can maintain strength and shield hydrogen bonds during compression.

Accordingly, this work differs from prior studies in terms of both the functional role of the introduced polymer network and the ultimate target performance. We have therefore added the following clarifications in the revised manuscript:

Revision: … Additionally, we developed a uniform polymer topological network

through in-situ polymerization and crosslinking, achieving the objective of maintaining fiber stiffness while effectively shielding inter-fiber hydrogen bonds. Following topological isomerization, the cellulose I aerogel yielded a cellulose III-based triboelectric aerogel (CNF-III@Si) that exhibits both superelasticity and high strength. (Manuscript, page 4-5, lines 84-89)

To more clearly elucidate the shielding mechanism of the polymer network, we have made the following revisions:

Revision: … The elasticity of cellulose aerogels is primarily attributed to the shielding effect of hydrogen bonds among the fibers. Previous studies indicate that chemical modification using silanes or petroleum-based polymers can effectively shield these hydrogen bonds, thereby improving elastic recovery[12,53]. In this context, uniform functionalization of the fiber surfaces is essential, as it directly influences the effectiveness of hydrogen bond shielding and ultimately impacts the material's elastic properties. (Manuscript, page 16-17, lines 316-321)

(ii) Hydrogen-bond disruption and the shielding mechanism of the polymer network

We understand and respect the reviewer's stringent criteria regarding whether a genuinely new principle or paradigm is introduced. In light of the reviewer's comments, we also recognize that the original manuscript did not sufficiently and precisely position the level of innovation of this work. It placed excessive emphasis on specific processing methods and performance improvements, while failing to adequately highlight the

underlying logic of structural regulation. As a result, the work could be perceived as merely an incremental optimization of existing approaches. Based on this understanding, we have carried out a systematic revision of the manuscript and added substantial experimental evidence to elucidate the mechanisms of hydrogen-bond disruption and polymer-network shielding:

① Hydrogen-bond disruption

We have deepened the discussion on how ethylenediamine-induced crystal transformation and the associated hydrogen-bond disruption affect the reactivity of cellulosic aerogels. Specifically, we added static water adsorption experiments (Supplementary Fig. 9) to directly compare the water-binding ability of CNF-I and CNF-III aerogels. Under identical conditions, CNF-III exhibits a significantly higher moisture-adsorption capacity, further confirming that hydrogen-bond disruption is beneficial for increasing hydroxyl accessibility in cellulosic aerogels. In addition, we supplemented macroscopic pore-size distribution data to demonstrate that hydrogen-bond disruption does not compromise the porous architecture of the aerogel (Supplementary Fig. 2).

Revision: … Static moisture absorption tests further indicated that, in a moderate 70% humidity environment, CNF-III aerogel achieved equilibrium within 30 minutes, exhibiting an equilibrium water absorption rate of 24%, in contrast to only 5.7% for CNF-I (Supplementary Fig. 9). The substantial increase in water absorption by CNF-III suggests a significantly enhanced accessibility of its hydroxyl groups, along with a more relaxed hydrogen bond network. (Manuscript, page 14, lines 286-291)

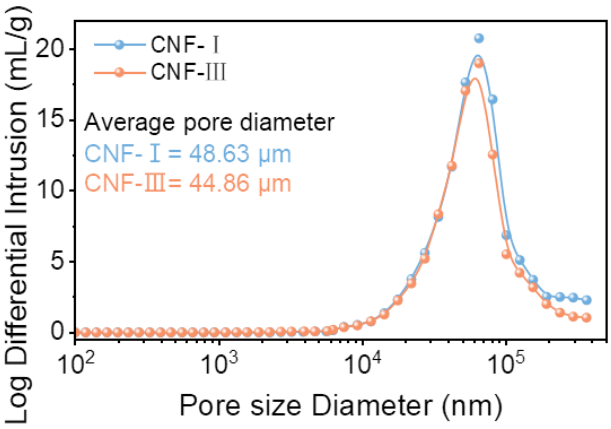

Supplementary Figure 2. Pore size distribution of CNF-I and CNF-III aerogels.

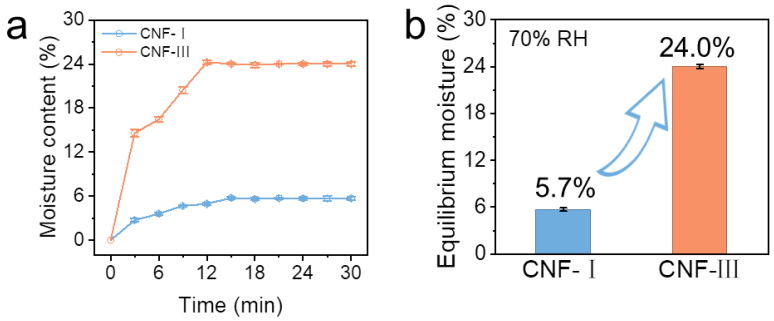

Supplementary Figure 9. Static moisture absorption test of CNF-I and CNF-III aerogels in saturated salt solution at 25 ℃ and 70% relative humidity. (**a**) Change in water content over time. (**b**) Equilibrium water content.

② Polymer network shielding mechanism

We sincerely thank the reviewer for the careful evaluation of the manuscript and for drawing attention to the issue of mechanistic novelty. The original version may not have sufficiently clarified the differences of this mechanism in terms of design hierarchy and functional intent, and we therefore wish to further elaborate here. In this work, the polymer network is not introduced as a conventional surface coating or a localized reinforcing phase. Instead, a continuous bulk topological network is constructed within the aerogel via *in situ* interfacial polymerization. This network fundamentally

reconstructs the inter-fiber connectivity topology (Fig. R4) as well as the electron transport pathways (Fig. R5). Beyond shielding hydrogen bonding, the topological network also plays a critical role in stabilizing the triboelectric output. Accordingly, both the target of action and the regulatory length scale of this mechanism differ from those of previously reported "network shielding" strategies.

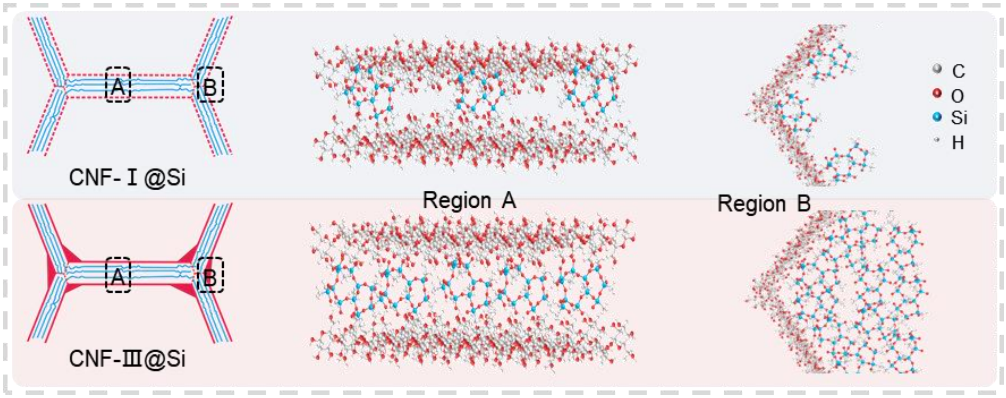

Figure R4. Schematic diagram of the reinforcement mechanism of the molecular network on the aerogel pore wall.

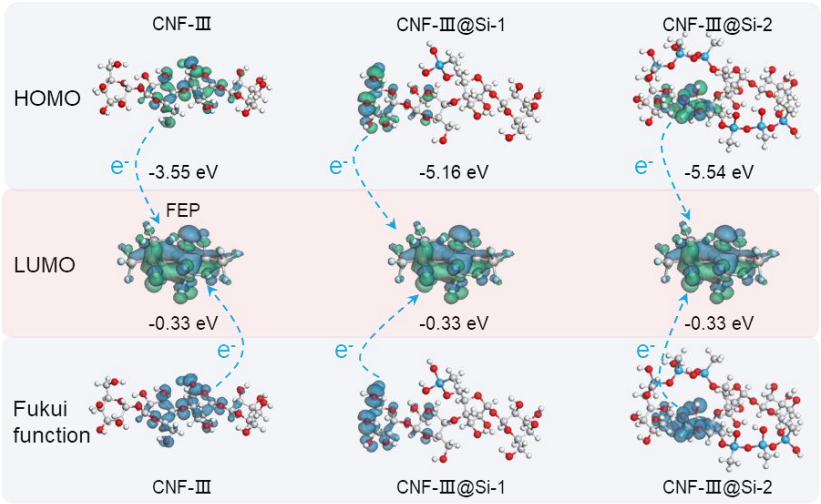

Figure R5. The highest occupied molecular orbital (HOMO) of CNF-III, CNF-III@Si-1, and CNF-III@Si-2 (top) and the distribution of electrophilic sites of the Fukui function (bottom), and the lowest unoccupied molecular orbital (LUMO) of FEP (center)

(A larger f-Fukui function value and a more concentrated HOMO distribution indicate a greater probability of electron loss).

More importantly, this bulk-phase topological reconstruction is not intended solely to enhance mechanical performance, but is deliberately employed to regulate triboelectric functionality. The crystal-structure rearrangement induced by topological isomerization, together with the cooperative constraint imposed by the polymer network, stabilizes the surface charge distribution (Fig. R6), thereby markedly suppressing charge dissipation and maintaining stable output over a wide range of temperatures and humidity (Fig. R7). We therefore believe that this mechanism does not represent a mere incremental optimization of existing approaches, but instead introduces a new design paradigm at the level of coupled regulation among bulk topological structure, mechanical behavior, and triboelectric output. This provides critical enabling conditions for the application of triboelectric aerogels in high-temperature and high-humidity environments.

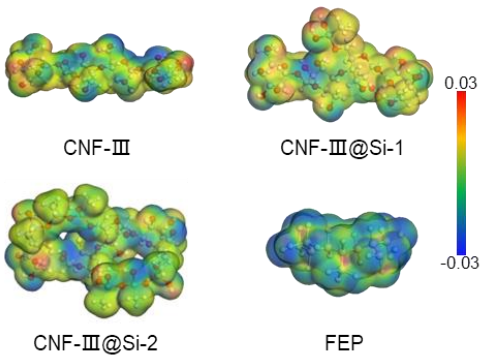

Figure R6. Electrostatic potential distributions of CNF-III, FEP, and two CNF-III@Si molecular models.

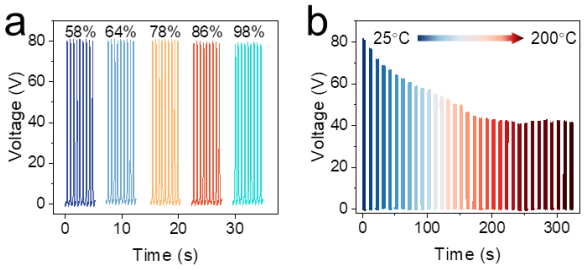

Figure R7. Output voltage at different humidity levels (**a**) and temperatures (**b**).

(iii) Evaluation of performance metrics

We thank the reviewer for the candid comments and would like to further clarify the performance design objectives and evaluation context that may not have been sufficiently articulated in the original manuscript. The aim of this study is not to maximize a single triboelectric output parameter, but rather to demonstrate performance stability and multidimensional synergy under complex environmental conditions, such as elevated temperature and high humidity.

The advantages of this work are reflected in the ability of the triboelectric output to remain stable over wide temperature and humidity ranges as well as under long-term cyclic operation. Accordingly, this study does not pursue transiently high output at the expense of stability, but instead offers a design strategy that balances overall performance with environmental adaptability. In the context of wearable sensing and applications in harsh or extreme environments, such stable output capability carries clear and independent scientific and engineering significance. To further substantiate this point, we have supplemented triboelectric nanogenerator output and energy-storage performance based on CNF-I@Si and CNF-III@Si aerogels, along with cyclic testing at different temperatures (25–200 °C), to demonstrate the excellent stability of the

triboelectric performance of these aerogels.

Revision: … Further investigation revealed that the CNF-III@Si aerogel–based TENG delivered a maximum output power density of 310 mW m^{-2}, nearly twice that of the CNF-I@Si aerogel (160 mW m^{-2}, Supplementary Fig. 26). It could charge a 0.1 μF capacitor to 12 V within 120 s, compared with only 2.1 V for the CNF-I@Si counterpart (Supplementary Fig. 26), demonstrating effective self-powered energy storage without external power input. The aerogel maintained stable output performance across a range of temperatures, including 25 °C, 50 °C, 75 °C, 100 °C, 150 °C, and 200 °C (Supplementary Fig. 27). (Manuscript, page 27, lines 520-527)

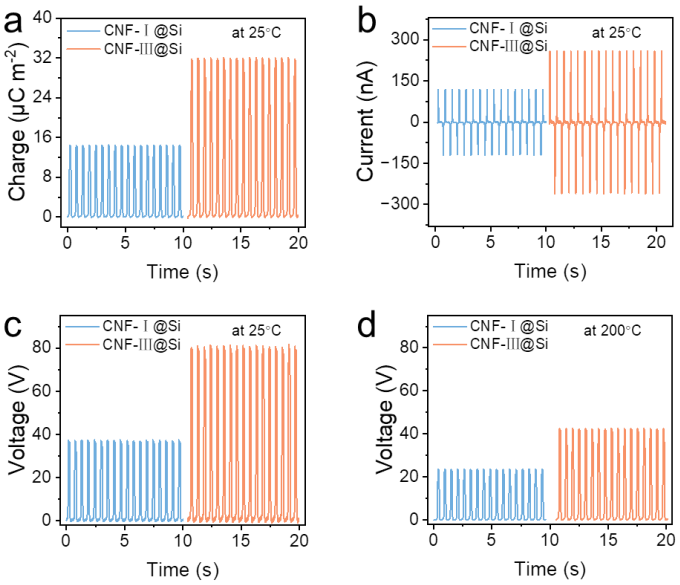

Supplementary Figure 23. Surface charge density (**a**), output current (**b**), and output voltage (**c**) of TENGs based on CNF-I@Si and CNF-III@Si aerogels at 25 °C. (**d**) Output voltage of TENGs based on CNF-I@Si and CNF-III@Si aerogels at 200 °C.

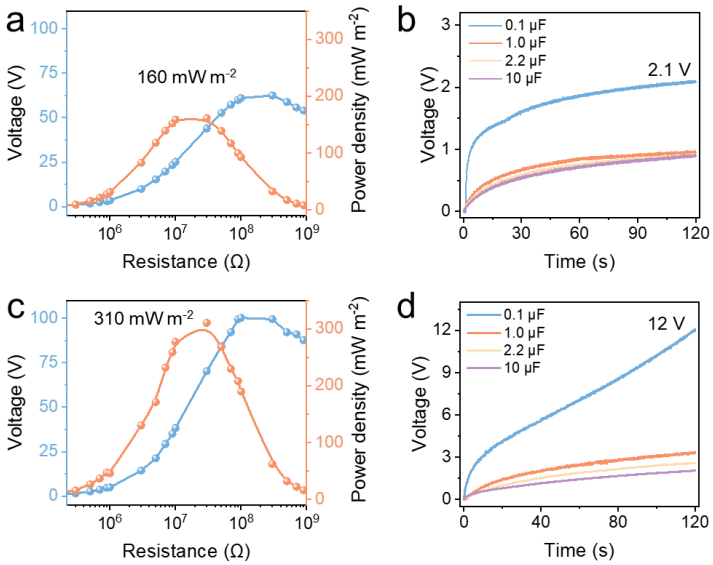

Supplementary Figure 26. (**a**) Output voltage and power density of the CNF-III@Si aerogel-based TENG under different external resistances. (**b**) Capacitor charging curve of the CNF-I@Si aerogel-based TENG. (**c**) Output voltage and power density of the CNF-III@Si aerogel-based TENG under different external resistances. (**d**) Capacitor charging curve of the CNF-III@Si aerogel-based TENG.

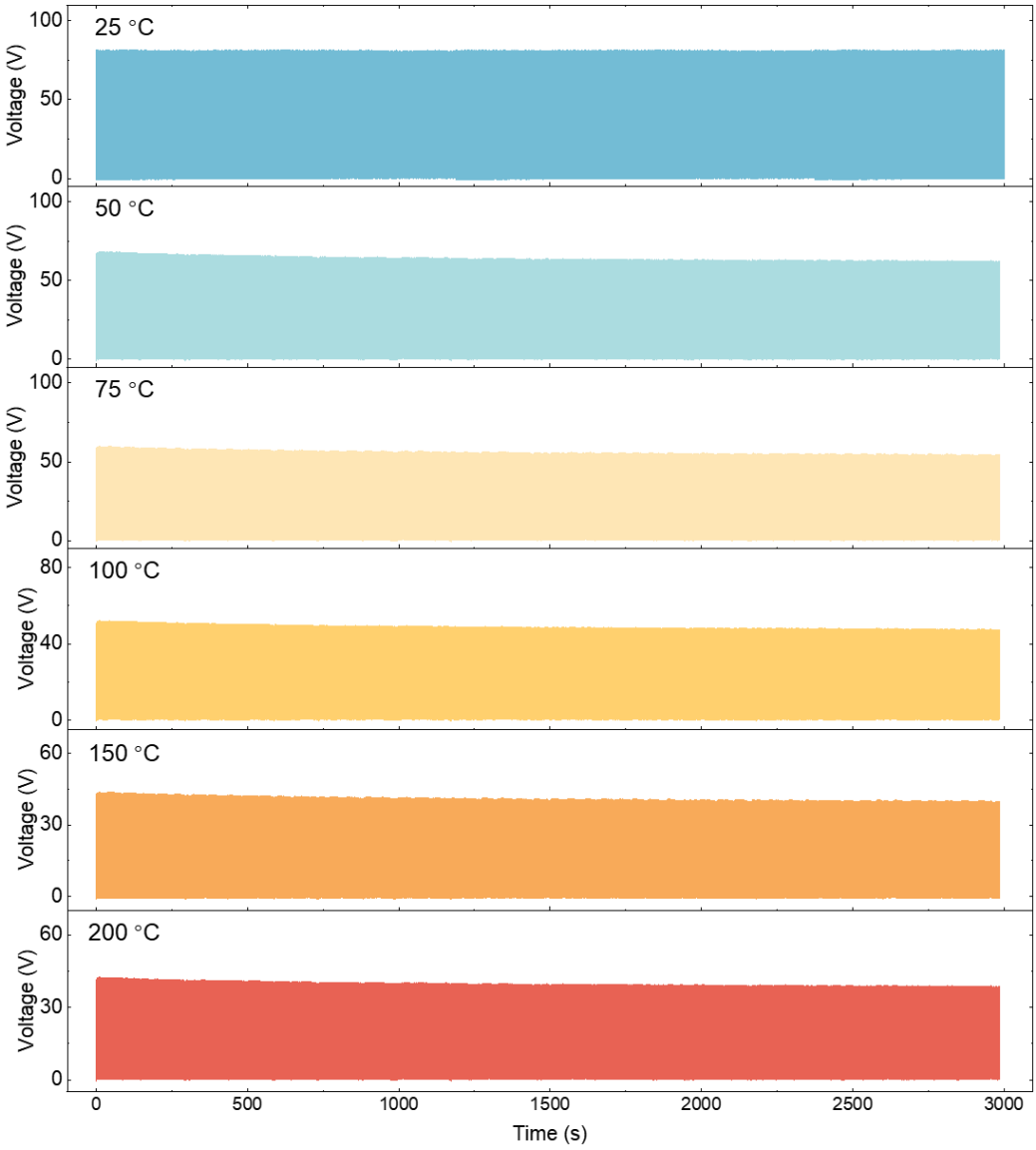

Supplementary Figure 27. The output voltage of TENG based on CNF-III@Si aerogel under cyclic testing at different temperatures, with a frequency of 2.0 Hz.

In addition, we surveyed a broad range of related studies and summarized representative works in Supplementary Table 1. As can be seen from this comparison, relative to other reported triboelectric aerogel materials, our aerogel exhibits advantages in terms of overall performance, including mechanical strength, elasticity, operating temperature range, and triboelectric output.

Supplementary Table 1. Summary of mechanical properties and triboelectric performance of triboelectric aerogels reported in the literature.

Materials	Elastic recovery rate (%)	Strength (kPa)	Max. working temperature (°C)	Contact area (cm^2)	V_{oc} (V)	Charge density ($\mu C/m^2$)	Power density ($mW\ m^{-2}$)	Ref.
ZZ-MSCA	38	17.5	-	9	120	48.88	70	13
CNF/PVA	0	2.8 MPa	45		60	67.5	265	14
AS/GO/PVA/CNF	75	155	-	135	34	0.59	-	15
CMPA	78.57%	320	-	4.9	72	97.5	270	16
hierarchical cellulose	95	55	100	529	320	70.89	310	17
TCNF/PVA/CNT	0	69.3	-	7	150	-	220	18
SCMC/CNC	-	130	50	8	132	-	-	19
CNF-III@Si	95	180.6	200	4	81.5	32	310	This work

Supplementary References

…

13. Su, J. *et al.* Superelastic Triboelectric Aerogel Enabled by Cross-Scale Fibers and Heterojunction Particles for Wearable Intelligent Neck Guard. *Adv. Funct. Mater.* **33**, e15065 (2025).

14. Luo, B. *et al.* Multiscale Structural Nanocellulosic Triboelectric Aerogels Induced by Hofmeister Effect. *Adv. Funct. Mater.* **33**, 2306810 (2023).

15. Wu, X. *et al.* Elastic Yet Strength Triboelectric Aerogel Enabled by Constructing a Supramolecular System. *Adv. Funct. Mater.* **35**, 2417067, (2024).

16. Meng, N. *et al.* Monolithic Conjugated Microporous Polymer Aerogel for Triboelectric Nanogenerator. *Adv. Funct. Mater.* **34**, 2313534 (2024).

17. Zhong, S. *et al.* Passive Isothermal Flexible Sensor Enabled by Smart Thermal-Regulating Aerogels. *Adv. Mater.* **37**, 2415386 (2025).

18. Gao, C. *et al.* Hierarchical porous triboelectric aerogels enabled by heterointerface engineering. *Nano Energy* **121**, 109223 (2024).

19. Cai, C. *et al.* Lightweight and Mechanically Robust Cellulosic Triboelectric Materials for Wearable Self-Powered Rehabilitation Training. *ACS Nano* **19**, 396–405 (2025).

We sincerely appreciate the reviewer's comments. We highly value and fully understand the reviewer's insights regarding the core concepts, underlying principles, and performance aspects of this study. We earnestly hope that the present revisions address the reviewer's concerns and clearly demonstrate the significance of our work in advancing the development of high-performance triboelectric aerogels.

Reviewer #2 (Remarks to the Author):

The manuscript introduces a topological isomerization approach that ingeniously reconciles the inherent conflict between strength and elasticity in cellulose aerogels.

Beyond its remarkable mechanical attributes, the aerogel also demonstrates consistent triboelectric efficacy, thereby presenting a cutting-edge material solution for self-powered flexible electronics. Overall, this is a meticulous and timely study. I believe it is suitable for publication in Nature Communications, with the following suggestions for improvement:

Response: We sincerely thank the reviewer for the careful evaluation of our manuscript and for the positive and constructive comments. We are pleased that the reviewer recognizes the significance of the proposed "topological isomerization" strategy in effectively addressing the inherent trade-off between mechanical strength and elasticity in cellulose aerogels, and its potential as an advanced material solution for self-powered flexible electronic devices.

We also appreciate the reviewer's valuable and specific suggestions, which are highly beneficial for improving the clarity, rigor, and overall quality of the manuscript. All comments have been carefully considered and addressed in the revised version.

1. The use of small-molecule ethylenediamine treatment to achieve cellulose crystal transformation in the aerogel state is a key aspect. It is recommended to design a reasonable control experiment to statistically analyze the changes in pore size distribution and pore wall morphology before and after treatment. This would better support the claim that the ethylenediamine treatment does not alter the microstructure of the aerogel.

Response: Thank you very much for pointing out this important issue. We fully agree

that more rigorous control experiments and quantitative statistical evidence are necessary to convincingly support the statement that ethylenediamine treatment does not significantly alter the microstructure of the aerogel.

To address this concern, mercury intrusion porosimetry was employed to quantitatively analyze the pore size distribution of the aerogels before and after ethylenediamine treatment. As shown in Supplementary Fig. 2, the pore size distributions remain nearly unchanged, with average pore diameters of 48.63 μm and 44.86 μm for the untreated and treated aerogels, respectively. In combination with the BET N_2 adsorption results (Supplementary Fig. 1) and the scanning electron microscopy observations (Supplementary Fig. 3), these results clearly demonstrate that the ethylenediamine treatment does not disrupt the intrinsic microstructure of the aerogel.

Revision: … Variations in N_2 adsorption and pore distribution indicate that the pore size of the micropores or mesopores remained largely unchanged (Supplementary Fig. 1 and 2). Additionally, SEM images reveal that the pore walls and structure were intact before and after ethylenediamine treatment (Supplementary Fig. 3). These pieces of evidence suggest that the treatment of CNF-I aerogel with EDA does not modify its three-dimensional pore architecture and maintains its original honeycomb porous structure. (Manuscript, page 6, lines 120-126)

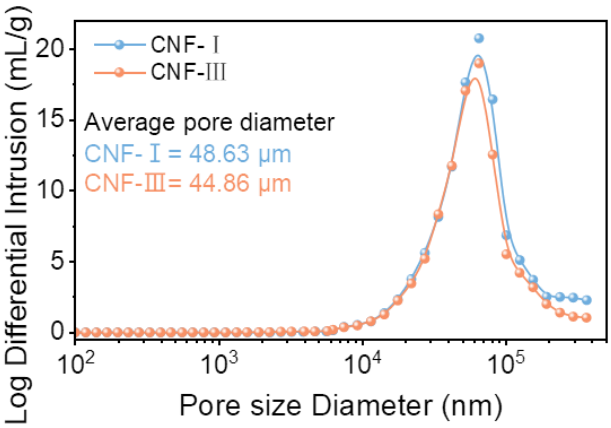

Supplementary Figure 2. Pore size distribution of CNF-I and CNF-III aerogels.

2. It is noted that ethylenediamine can be recycled and reused during the treatment process. Although this is illustrated in a figure, it should be explicitly mentioned in the main text, as it represents a unique advantage of this manuscript.

Response: Thank you for this helpful suggestion. We agree that the environmentally friendly and cost-effective nature of this approach is an important merit of the present work and should be explicitly stated in the main text rather than only illustrated schematically. Accordingly, we have revised the description of the ethylenediamine treatment process to clearly indicate that the ethylenediamine solution can be recovered via reduced-pressure distillation and reused in subsequent cycles.

Revision (1): … The EDA employed in this process can be recovered and reused via vacuum distillation, achieving a recovery rate of approximately 90%. (Manuscript, page 6, lines 118-120)

Revision (2): … The aerogel was then air-dried at room temperature to a constant weight, and the resulting CNF III aerogel was sealed and stored in a desiccator for future use. The treated EDA can be recovered through vacuum distillation. (Manuscript,

page 31, lines 587-590)

3. The authors constructed a polymer topological network in the aerogel via in-situ polymerization, but the manuscript only shows the elemental distribution of C, O, and Si for CNF-III@Si. Including the corresponding data for CNF-I@Si would better demonstrate the beneficial effect of the pretreatment on the in-situ polymerization.

Response: This is a very helpful and insightful suggestion. We agree that a direct comparison of the elemental distributions between CNF-I@Si and CNF-III@Si can more clearly demonstrate the beneficial effect of the ethylenediamine pretreatment—by increasing hydroxyl accessibility—on the uniformity and effectiveness of the subsequent in situ interfacial polymerization.

Accordingly, we have added EDS elemental mapping analyses of CNF-I@Si aerogels prepared via direct in situ polymerization without ethylenediamine pretreatment. A comparative discussion of these results has been included in the main text. Notably, the CNF-III@Si sample exhibits a more homogeneous and intense Si distribution, providing direct evidence that the pretreatment plays a critical role in constructing a uniform and dense polymer topological network.

Revision: As shown in Fig. 3e and Supplementary Fig.11, both CNF-I@Si and CNF-III@Si aerogels possess smooth pore walls. However, a comparison of the silicon element distribution via EDS indicates that the pore walls of the CNF-III@Si aerogel are enveloped by a more uniform and denser polymer network. (Manuscript, page 18-19, lines 349-352)

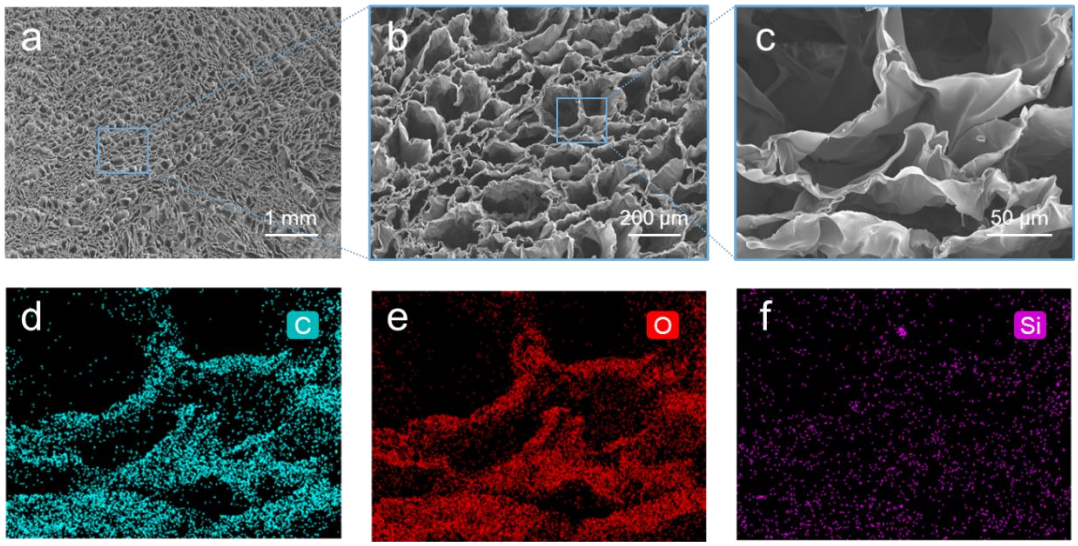

Supplementary Figure 11. (**a-c**) SEM images of CNF-I@Si aerogel. (**b**) and (**c**) are magnified local images of (**a**) and (**b**), respectively. (**d-f**) EDS elemental distribution based on (**c**): (**d**) C, (**e**) O, (**f**) Si.

4. It is recommended to supplement the analysis of the pore size distribution of CNF-III@Si aerogels before and after compression to illustrate the structural stability of the aerogel.

Response: Thank you very much for this important suggestion. We agree that analyzing the pore size distribution of CNF-III@Si aerogels before and after compression cycles provides one of the most direct microstructural evidences for evaluating their structural stability and excellent elastic recovery.

Accordingly, mercury intrusion porosimetry was employed to characterize the pore size distribution of the aerogels after multiple compression cycles and to compare it with that of the pristine (uncompressed) samples. The results show a slight decrease in the average pore size after repeated compression, which can be attributed to a recoverable

densification of the porous framework under mechanical loading, while the overall pore structure remains well preserved.

Revision: … The average pore diameter decreased by approximately 7.5 μm before and after cyclic compression, with no significant change in pore distribution, indicating that the aerogel's pore structure maintained substantial integrity (Supplementary Fig. 18). (Manuscript, page 21, lines 410-413)

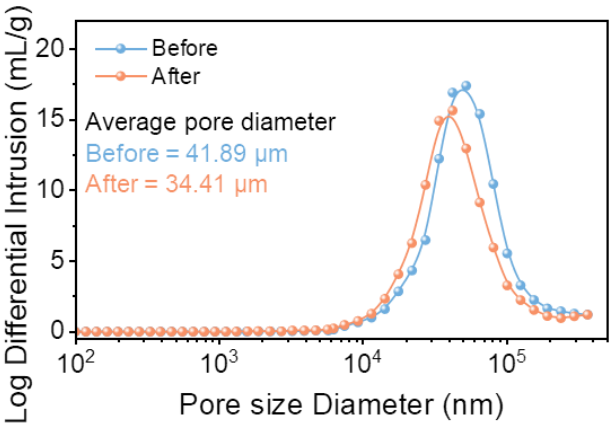

Supplementary Figure 18. Pore diameter distribution of CNF-III@Si before and after cyclic compression.

5. The molecular structure of CNF-III@Si shown in Figure 3d appears to differ from that in Figure 1a. The currently depicted siloxane linkages between cellulose chains do not fall within the category of polymers and should be appropriately corrected.

Response: We sincerely thank the reviewer for the careful examination of the figures and for pointing out the inaccuracy in the structural representation. The reviewer is absolutely correct that the siloxane linkages (–Si–O–Si–) currently depicted in Fig. 3d correspond to small-molecule crosslinking points and do not appropriately represent a

polymeric topology network, nor are they fully consistent with the molecular structure shown in Fig. 1a.

In response to this comment, Fig. 3d has been redrawn to accurately illustrate the polymer chains formed via in situ polymerization and their topological interconnection among the cellulose nanofibers, thereby ensuring conceptual and structural consistency throughout the manuscript.

Revision:

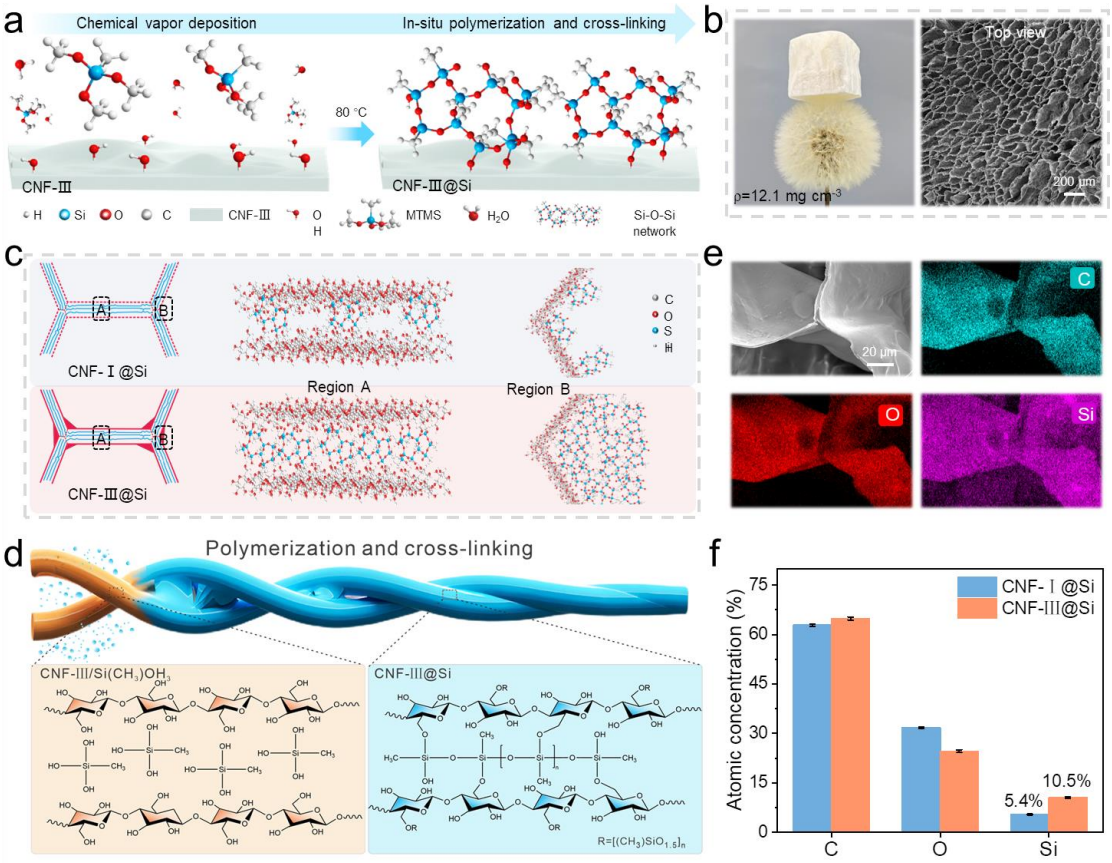

Figure 3. Vapor-mediated in situ interfacial polymerization and covalent crosslinking. (**a**) Covalent bonding of the silane network to cellulose via vapor deposition. (**b**) Digital image (left) and surface SEM image (right) of CNF-III@Si aerogel. (**c**) Schematic diagram of the reinforcement mechanism of the molecular network on the aerogel pore wall. (**d**) In situ hydrolysis and polycondensation of MTMS

result in a uniform polymer coating on the fiber surface. (**e**) SEM image and EDS elemental distribution of the pore wall of CNF-III@Si aerogel. (**f**) Comparison of elemental content between CNF-I@Si and CNF-III@Si aerogels.

6. The topological isomerization strategy enables the CNF-III@Si aerogel to achieve ultra-high elasticity and high strength. The authors provided a detailed analysis of the mechanical performance after 20,000 compression cycles. However, structural changes in aerogels often occur during the initial compression cycles. Therefore, it is recommended that the authors supplement the analysis of the first 500 compression cycles to fully demonstrate the structural stability of the aerogel.

Response: This is a very important point. We agree that the mechanical response of aerogels during the initial compression cycles can strongly influence their subsequent cyclic stability, and that analyzing the early-stage behavior allows for a more comprehensive evaluation of structural robustness.

In response to this suggestion, in addition to the 20,000-cycle long-term compression data, we have supplemented a mechanical analysis focusing on the first 500 compression cycles. This analysis specifically examines the evolution of plastic deformation, compressive strength, and elastic recovery during the early cycling stage. The results show that after limited structural adjustment in the initial cycles, both the strength and elasticity of the CNF-III@Si aerogel quickly reach a stable state, demonstrating its excellent structural stability.

Revision: … During the initial 500 cycles of compression, CNF-I@Si aerogel

demonstrated considerable plastic deformation, whereas CNF-III@Si aerogel exhibited less than 2% plastic deformation (Supplementary Fig. 15 b-d). After 20,000 cycles of compression at 50% strain, the maximum strength of CNF-III@Si aerogel was maintained at 108.5 kPa, with its geometric height and shape remaining nearly unchanged (Fig. 4d). The observed decrease in strength is likely attributable to the accumulation of damage at the microstructural level, including skeletal bending, node rearrangement, or progressive interface fatigue, rather than an overall structural collapse. (Manuscript, page 20-21, lines 393-401)

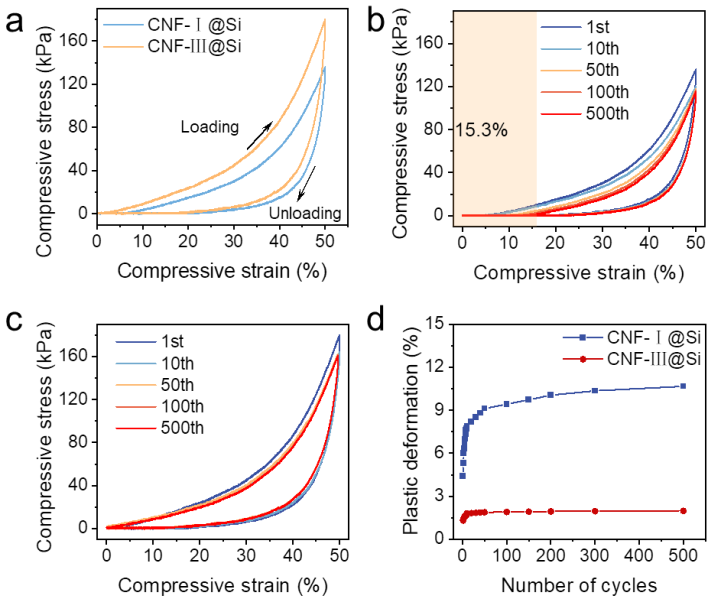

Supplementary Figure 15. (**a**) Stress-strain curves of CNF-I@Si and CNF-III@Si aerogels. Stress-strain curves of CNF-I@Si (**b**) and CNF-III@Si aerogels (**c**) for the first 500 cycles of compression. (**d**) Plastic deformation of CNF-I@Si and CNF-III@Si aerogels for the 500 cycles of compression.

7. To more fully demonstrate the stability of the aerogel's triboelectric performance, it is suggested that the authors supplement cyclic tests at different temperatures, such as

50 °C, 100 °C and 150 °C, which would better illustrate the superiority of the aerogel's performance.

Response: Thank you for this valuable suggestion aimed at further strengthening the validation of the triboelectric performance. We agree that supplementing cyclic stability tests at elevated temperatures is important for demonstrating the robustness of the aerogel under extreme thermal conditions.

In response, we have conducted additional triboelectric output stability tests of the CNF-III@Si aerogel at 25 °C, 50 °C, 75 °C, 100 °C, 150 °C, and 200 °C, with a testing frequency of 2 Hz. As shown by the results, the output voltage remains highly stable across the entire temperature range, with the deviation of the initial signal amplitude remaining below 2% at all tested temperatures. These results clearly demonstrate the superior triboelectric stability of the aerogel over a wide temperature window.

Revision: … The aerogel maintained stable output performance across a range of temperatures, including 25 °C, 50 °C, 75 °C, 100 °C, 150 °C, and 200 °C (Supplementary Fig. 27). (Manuscript, page 27, lines 525-527)

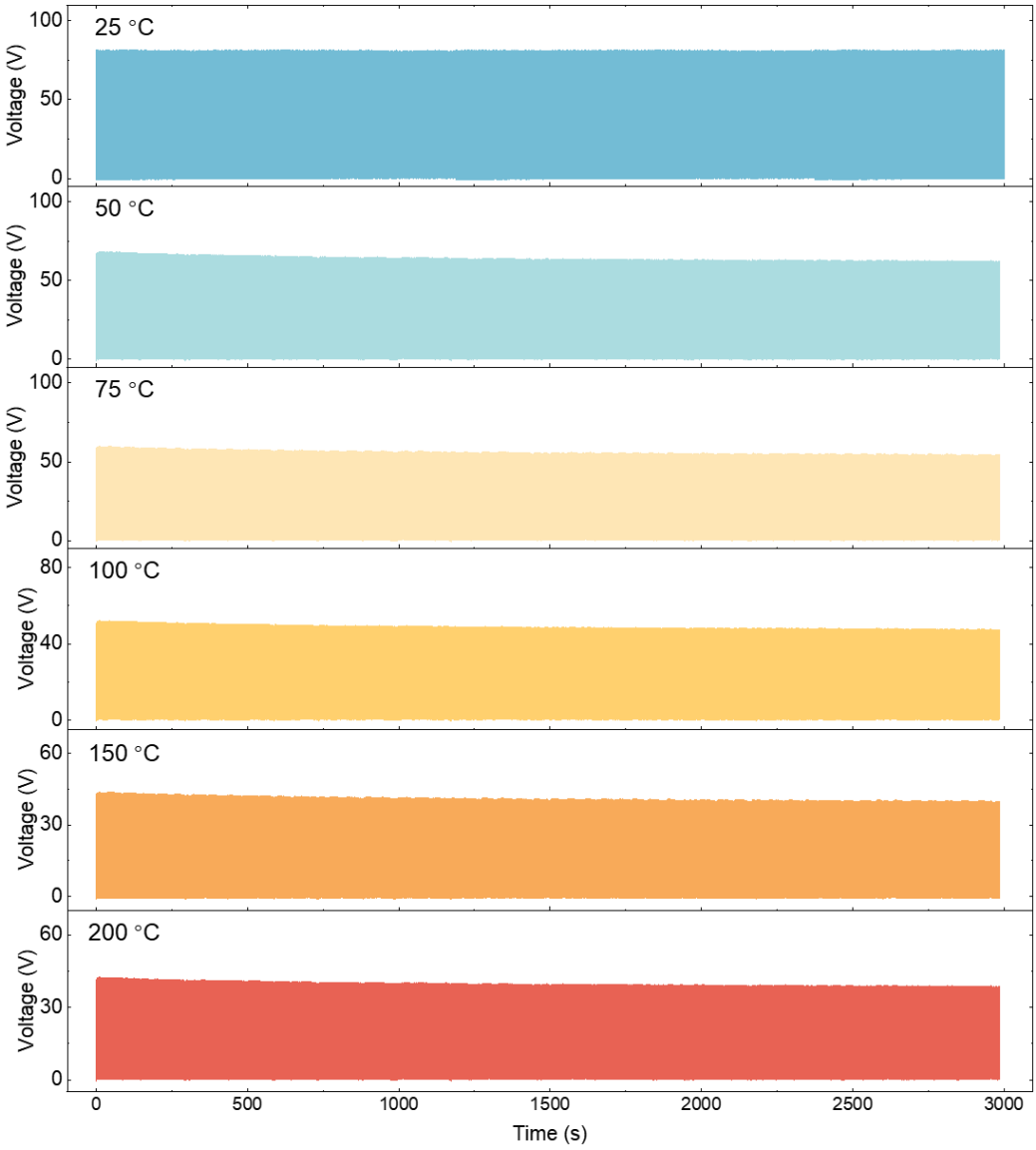

Supplementary Figure 27. The output voltage of TENG based on CNF-III@Si aerogel under cyclic testing at different temperatures, with a frequency of 2 Hz.

8. Although CNF-I@Si aerogels do not exhibit mechanical properties as excellent as those of CNF-III@Si, the manuscript lacks a comparison of their triboelectric output performance.

Response: We agree that this is an important and necessary control experiment. In response to this comment, we have supplemented the triboelectric output performance

of CNF-I@Si aerogels measured under the same testing conditions, including the open-circuit voltage, short-circuit current, and transferred charge. A direct comparison with CNF-III@Si is now provided, allowing for a more comprehensive evaluation of the differences in triboelectric performance between the two aerogels.

Revision: … Supplementary Fig. 23 illustrates a comparison of the triboelectric output performance between CNF-I@Si and CNF-III@Si aerogels. At 25 °C, the surface charge density, output current, and voltage of the TENG based on the CNF-III@Si aerogel surpass those of the CNF-I@Si variant. Conversely, at elevated temperatures of 200 °C, the output voltage of the CNF-I@Si aerogel-based TENG experiences a significant decline, whereas the output voltage of the CNF-III@Si aerogel-based TENG remains stable at 41.6 V. The mechanical nonlinear behavior of porous elastomer materials results in a sensing hysteresis phenomenon in the signal curve. Further testing assessed the output performance under varying compressive strengths. (Manuscript, page 26-27, lines 501-509)

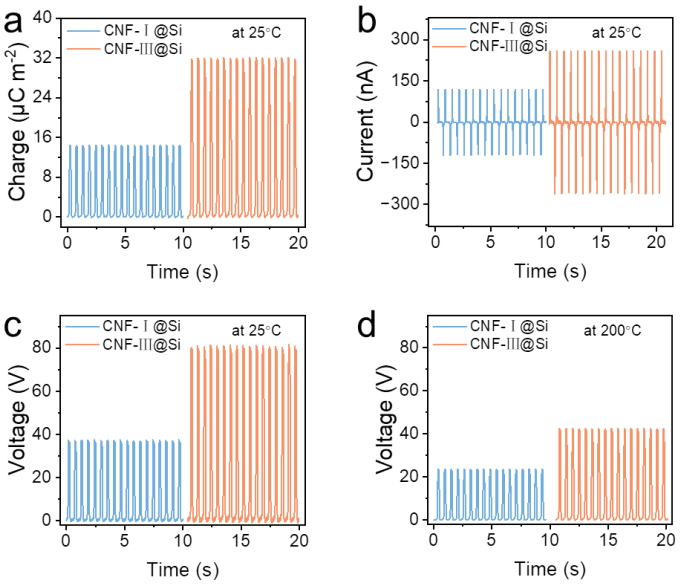

Supplementary Figure 23. Surface charge density (**a**), output current (**b**), and output voltage (**c**) of TENGs based on CNF-I@Si and CNF-III@Si aerogels at 25 °C. (**d**) Output voltage of TENGs based on CNF-I@Si and CNF-III@Si aerogels at 200 °C.

9. Power density is an important reference data for evaluating triboelectric performance. It is recommended that the authors supplement relevant data on power density.

Response: Thank you for pointing out this important performance metric. We agree that power density is a critical parameter for evaluating the triboelectric performance. In response to this comment, we have supplemented the power density analysis of the CNF-III@Si triboelectric aerogel.

As shown in Supplementary Fig. 26a, the output voltage was systematically measured under different external load resistances, and the instantaneous power density was calculated and plotted as a function of the load resistance. The results indicate that the maximum output power is achieved at a load resistance of approximately 2×10^7 Ω, corresponding to a peak power density of 310 mW m^{-2}.

In addition, the charging capability of the triboelectric aerogel was further evaluated. The device is able to charge a 0.1 μF capacitor to 12 V within 120 s, clearly demonstrating its effective energy output and storage potential.

Revision: … Further investigation revealed that the CNF-III@Si aerogel–based TENG delivered a maximum output power density of 310 mW m^{-2}, nearly twice that of the CNF-I@Si aerogel (160 mW m^{-2}, Supplementary Fig. 26). It could charge a 0.1 μF capacitor to 12 V within 120 s, compared with only 2.1 V for the CNF-I@Si counterpart

(Supplementary Fig. 26), demonstrating effective self-powered energy storage without external power input. (Manuscript, page 27, lines 520-525)

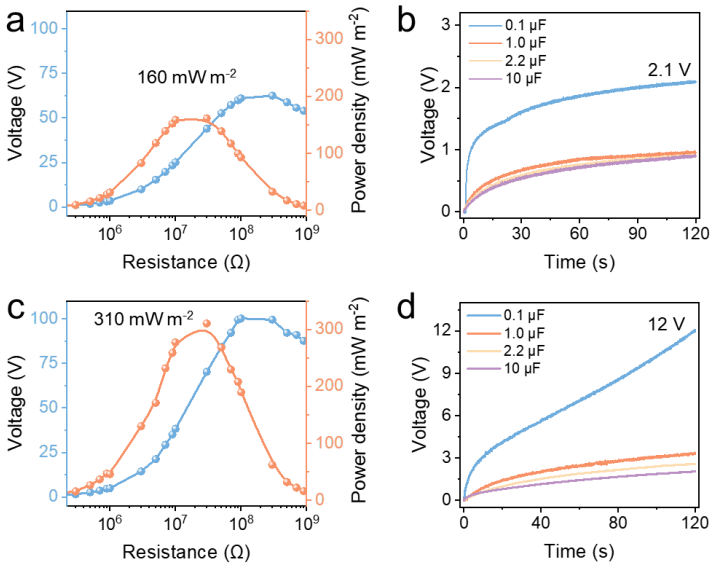

Supplementary Figure 26. (**a**) Output voltage and power density of the CNF-III@Si aerogel-based TENG under different external resistances. (**b**) Capacitor charging curve of the CNF-I@Si aerogel-based TENG. (**c**) Output voltage and power density of the CNF-III@Si aerogel-based TENG under different external resistances. (**d**) Capacitor charging curve of the CNF-III@Si aerogel-based TENG.

10. The authors claim that the CNF-III@Si triboelectric aerogel exhibits significant environmental tolerance. This should be supported by comparing its performance with other similar aerogels.

Response: We fully agree that placing the performance of the present material in a broader literature context is essential for objectively demonstrating its environmental tolerance.

In response to this comment, we have conducted a systematic survey of recently

reported triboelectric materials with excellent environmental stability, particularly those exhibiting high tolerance to humidity and temperature, with an emphasis on cellulose-based and polymer-based aerogels. A comparative summary is now provided in Supplementary Table S1, where the CNF-III@Si aerogel developed in this work is benchmarked against representative state-of-the-art materials in terms of material type, operational temperature and humidity ranges, output stability, and mechanical resilience. This comparison clearly highlights the competitive advantages of the present aerogel.

Revision: … Compared to other reported triboelectric aerogels (Supplementary Table 1), CNF-III@Si aerogel has advantages in mechanical properties, high temperature resistance, and triboelectric properties, showing its excellent application potential. (Manuscript, page 7, lines 140-143)

Supplementary Table 1. Summary of mechanical properties and triboelectric performance of triboelectric aerogels reported in the literature.

Materials	Elastic recovery rate (%)	Strength (kPa)	Max. working temperature (°C)	Contact area (cm^2)	V_{oc} (V)	Charge density ($\mu C/m^2$)	Power density ($mW\ m^{-2}$)	Ref.
ZZ-MSCA	38	17.5	-	9	120	48.88	70	13
CNF/PVA	0	2.8 MPa	45		60	67.5	265	14
AS/GO/PVA/CNF	75	155	-	135	34	0.59	-	15

CMPA	78.57%	320	-	4.9	72	97.5	270	16
hierarchical cellulose	95	55	100	529	320	70.89	310	17
TCNF/PVA/CNT	0	69.3	-	7	150	-	220	18
SCMC/CNC	-	130	50	8	132	-	-	19
CNF-III@Si	95	180.6	200	4	81.5	32	310	This work

Supplementary References

…

13. Su, J. *et al.* Superelastic Triboelectric Aerogel Enabled by Cross-Scale Fibers and Heterojunction Particles for Wearable Intelligent Neck Guard. *Adv. Funct. Mater.* **33**, e15065 (2025).

14. Luo, B. *et al.* Multiscale Structural Nanocellulosic Triboelectric Aerogels Induced by Hofmeister Effect. *Adv. Funct. Mater.* **33**, 2306810 (2023).

15. Wu, X. *et al.* Elastic Yet Strength Triboelectric Aerogel Enabled by Constructing a Supramolecular System. *Adv. Funct. Mater.* **35**, 2417067, (2024).

16. Meng, N. *et al.* Monolithic Conjugated Microporous Polymer Aerogel for Triboelectric Nanogenerator. *Adv. Funct. Mater.* **34**, 2313534 (2024).

17. Zhong, S. *et al.* Passive Isothermal Flexible Sensor Enabled by Smart Thermal-Regulating Aerogels. *Adv. Mater.* **37**, 2415386 (2025).

18. Gao, C. *et al.* Hierarchical porous triboelectric aerogels enabled by heterointerface

engineering. *Nano Energy* **121**, 109223 (2024).

19. Cai, C. *et al.* Lightweight and Mechanically Robust Cellulosic Triboelectric Materials for Wearable Self-Powered Rehabilitation Training. *ACS Nano* **19**, 396–405 (2025).

11. Another important aspect of triboelectric performance is energy storage capacity. It is suggested to include a comparative analysis of the energy storage capabilities of CNF-I@Si and CNF-III@Si aerogels.

Response: This is a very insightful and constructive suggestion. To comparatively evaluate the energy storage capabilities of CNF-I@Si and CNF-III@Si aerogels, we performed controlled capacitor-charging experiments under strictly identical testing conditions. Specifically, CNF-I@Si and CNF-III@Si aerogels with the same effective area were used as the triboelectric layers, operated at the same working frequency and applied pressure, and connected to a capacitor with a fixed capacitance.

The comparative charging results are presented as supplementary figures (e.g., Supplementary Fig. 26) and are discussed in the main text.

Revision: … Further investigation revealed that the CNF-III@Si aerogel–based TENG delivered a maximum output power density of 310 mW m^{-2}, nearly twice that of the CNF-I@Si aerogel (160 mW m^{-2}, Supplementary Fig. 26). It could charge a 0.1 μF capacitor to 12 V within 120 s, compared with only 2.1 V for the CNF-I@Si counterpart (Supplementary Fig. 26), demonstrating effective self-powered energy storage without external power input. (Manuscript, page 27, lines 520-527)

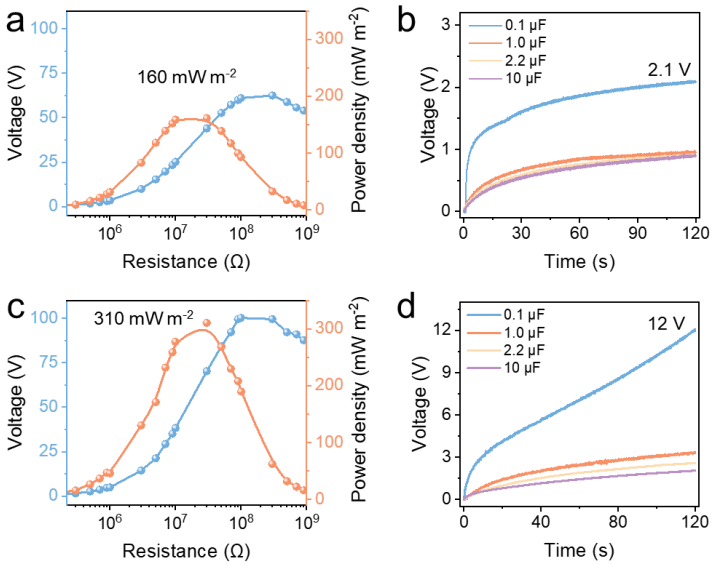

Supplementary Figure 26. (**a**) Output voltage and power density of the CNF-III@Si aerogel-based TENG under different external resistances. (**b**) Capacitor charging curve of the CNF-I@Si aerogel-based TENG. (**c**) Output voltage and power density of the CNF-III@Si aerogel-based TENG under different external resistances. (**d**) Capacitor charging curve of the CNF-III@Si aerogel-based TENG.

Reviewer #3 (Remarks to the Author):

This work described an interesting topological isomerization strategy in which ethylenediamine treatment induced the transformation of cellulose I to cellulose III, significantly enhancing the hydroxyl accessibility and reactivity of the aerogels. Building on this, an in-situ polymerization approach was used to construct a uniform polymer topological network, enabling the fabrication of cellulose aerogels that combine super elasticity, high mechanical strength, and stable triboelectric output. The material exhibited excellent performance even under extreme temperature and humidity conditions, offering a new paradigm for the development of flexible electronic devices.

I recommend acceptance of the manuscript for publication after addressing the following revision comments.

Response: We sincerely thank the reviewer for the careful evaluation of our manuscript and for the highly positive and constructive comments. We are pleased that the reviewer finds the proposed "topological isomerization" strategy interesting, and recognizes that the ethylenediamine-induced transformation from cellulose I to cellulose III—enhancing hydroxyl accessibility and reactivity—combined with in situ polymerization to construct a uniform polymer topological network, provides a new paradigm for fabricating cellulose aerogels that simultaneously exhibit super elasticity, high mechanical strength, and stable triboelectric output.

We are also encouraged by the reviewer's recognition of the excellent performance of the material under extreme temperature and humidity conditions, as well as its potential for flexible electronic devices. We fully agree with all the revision comments provided. These valuable suggestions have helped us further improve the experimental evidence, deepen the mechanistic discussion, and enhance the clarity and rigor of the manuscript. All comments have been carefully addressed and incorporated into the revised version.

1. This work have thoroughly characterized the microporous structure of the aerogels using SEM, BET, and other techniques, clearly revealing their honeycomb-like morphology and specific surface area features. However, providing additional insight into how the topological isomerization influences pore orientation or nanoscale ordering would further enhance the rigor of the manuscript.

Response: Thank you very much for this insightful and constructive suggestion. We agree that, beyond SEM and BET analyses, additional characterization is necessary to elucidate how the topological isomerization influences pore orientation and nanoscale ordering in the aerogels. To address this point and further strengthen the structural analysis, small-angle X-ray scattering (SAXS) measurements were performed.

By analyzing the characteristic features in the one-dimensional scattering profiles as well as the anisotropy in the two-dimensional SAXS patterns, we evaluated the evolution of the orientation of cellulose nanofiber bundles and pore walls during the topological isomerization process. As shown in the 2D SAXS patterns of the CNF-III@Si aerogels (Supplementary Fig. 12a), pronounced anisotropic scattering with elongated streaks along a specific direction is observed, indicating that the aerogel preserves the oriented architecture induced by directional ice-crystal growth during freeze casting at the macroscopic scale.

This orientation is further confirmed by the azimuthal intensity distribution, where a stronger scattering intensity appears at $\theta = 90°$ (Supplementary Fig. 12b). In addition, the Herman's orientation factor (f) was calculated to quantitatively assess the degree of ordering. In principle, $f = -0.5$ corresponds to complete alignment of crystal planes parallel to the reference direction (fully anisotropic), whereas $f = 0$ indicates random orientation (isotropic). The calculated f value of -0.394 for the CNF-III@Si aerogel demonstrates a pronounced structural orientation resulting from the combined effects of directional freezing and topological isomerization.

Revision: … The two-dimensional small-angle X-ray scattering (2D-SAXS) pattern of

CNF-III@Si exhibits pronounced anisotropic scattering features, accompanied by stripe-like scattering that is elongated in a specific direction (Supplementary Fig.12a). This observation suggests that the aerogel preserves the orientation structure induced by ice crystal growth during directional freezing on a macroscopic scale, as evidenced by a Herman's orientation factor of -0.394 (Supplementary Fig. 12b). (Manuscript, page 19, lines 353-359)

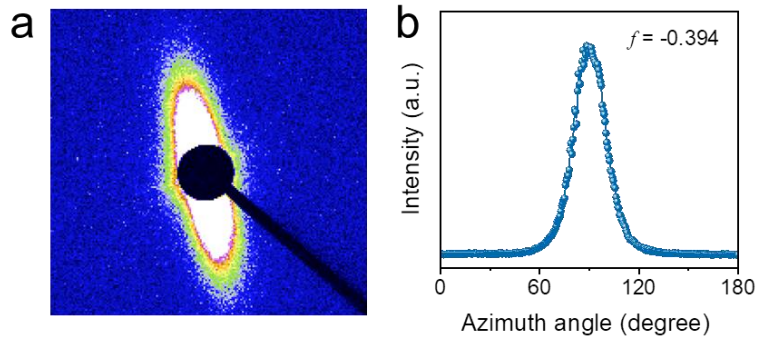

Supplementary Figure 12. 2D SAXS pattern (**a**) and Azimuthal plot (**b**) of CNF-III@Si aerogel. The formula for calculating the Hermann orientation factor (f) is as follows [12]:

$$f = \frac{3(cos^2\varphi)-1}{2} \quad (7)$$

where $(\cos^2\varphi)$ denotes the average of the squares of the cosine function of the azimuth angle from 0 to π/2, and its calculation formula is:

$$(cos^2\varphi) = \frac{\int_0^{\frac{\pi}{2}} I(\varphi)cos^2\varphi \sin\varphi d\varphi}{\int_0^{\frac{\pi}{2}} I(\varphi)sin\ \varphi d\varphi} \quad (8)$$

where $I(\varphi)$ is the intensity at azimuth angle φ. The computed value of f is -0.394, suggesting that the aerogel demonstrates a distinct structural orientation following directional freezing.

2. It stated that silanization enhances thermal stability, but it lacks an analysis of how the Si–O covalent network contributes to the thermal decomposition behavior. It is recommended that the authors further interpret the protective effect of the Si–O network based on the TGA/DTG results.

Response: Thank you for this insightful comment regarding the thermal decomposition behavior of silanized CNF-III and the role of the Si–O covalent network. We agree that a more detailed interpretation of the protective effect of the Si–O network based on the TGA/DTG results is necessary.

As revealed by the TGA/DTG curves (Supplementary Fig. 20), the thermal decomposition of CNF-III@Si after vapor-phase silanization is clearly shifted toward higher temperatures, accompanied by an increased residual mass at elevated temperatures, indicating an enhanced thermal stability. This improvement can be attributed to the condensation reactions between the surface hydroxyl groups of cellulose and methyltrimethoxysilane, leading to the formation of covalently bonded Si–O–C and Si–O–Si networks throughout the aerogel framework.

Owing to the high bond energy and excellent thermal stability of Si–O bonds, this inorganic–organic hybrid network remains structurally stable within the temperature range of cellulose decomposition, thereby effectively suppressing chain scission and the release of volatile fragments during heating. In addition, the interconnected Si–O network acts as a protective barrier that impedes heat and mass transfer, while promoting the formation of a silicon-rich char layer at high temperatures. This effect further retards thermal degradation and is consistent with the increased char yield

observed in the TGA results.

Taken together, these results indicate that although ethylenediamine-induced topological isomerization reduces the intrinsic thermal stability of cellulose III by lowering crystallinity and weakening hydrogen-bond interactions, the subsequent construction of a surface-crosslinked topological polymer network introduces thermally robust Si–O covalent structures that effectively compensate for this effect, resulting in an overall increase in decomposition temperature and high-temperature stability.

Revision: … In the radial direction, although heat flow frequently intersects with pore walls and fiber connections, the low solid volume fraction and numerous gas-solid interfaces limit effective phonon transport. Therefore, bidirectional heat transfer is primarily governed by gas-phase conduction and interfacial scattering, rather than a discontinuous solid-phase thermal path, resulting in comparable axial and radial thermal conductivity values. Thermogravimetric analysis (TGA) indicates that the thermal degradation temperature of CNF-III@Si reaches 290 °C (Supplementary Fig. 20). (Manuscript, page 22, lines 424-431)

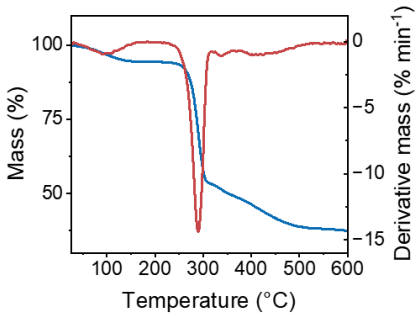

Supplementary Figure 20. TG and DTG curves of CNF-III@Si aerogel.

3. The discussion of hydrogen-bond network relaxation in CNF-III was primarily

supported by molecular dynamics–derived hydrogen-bond statistics (Figure 2c) and deconvolution of FTIR hydroxyl peaks (Figure 2d–e), which provided only indirect evidence of hydrogen-bond weakening. Direct experimental characterization of hydrogen-bond energy changes or conformational transitions would more convincingly support the core mechanistic pathway of "hydrogen-bond weakening → chain relaxation → altered thermal decomposition behavior."

Response: Thank you for this insightful and critical comment. We agree that hydrogen-bond weakening inferred from molecular dynamics–derived hydrogen-bond statistics and FTIR hydroxyl peak deconvolution mainly provides indirect evidence. To more convincingly support the proposed mechanistic pathway, we have supplemented direct experimental characterization by introducing static water vapor adsorption measurements, which can directly probe hydroxyl accessibility and the openness of the hydrogen-bond network in the aerogels.

Specifically, CNF-I and CNF-III aerogels were placed in sealed desiccators containing saturated NaCl solution (25 °C, corresponding to a relative humidity of 70% ± 5%), and their moisture adsorption behaviors are shown in Supplementary Fig. 9. Although both aerogels exhibit a gradual increase in water uptake during the initial 12 min, their equilibrium moisture contents differ markedly. At 70% RH, CNF-I reaches an equilibrium moisture content of only 5.7%, whereas CNF-III shows a significantly higher value of 24.0%. The substantially enhanced water uptake of CNF-III directly indicates increased hydroxyl accessibility and a more relaxed hydrogen-bond network. This trend is fully consistent with the FTIR hydroxyl band analysis, the conformational

transitions observed by solid-state NMR, and the faster dynamic wetting behavior revealed by water contact angle measurements. Together, these results provide converging experimental evidence that hydrogen-bond interactions in CNF-III are weaker than those in CNF-I, leading to increased exposure of reactive hydroxyl groups. Furthermore, TG/DTG analysis shows that CNF-III exhibits a noticeably lower thermal degradation temperature than CNF-I, corroborating the reduced hydrogen-bond energy and enhanced chain flexibility inferred from the water vapor adsorption behavior.

Taken together, the combined results from static moisture adsorption, FTIR, solid-state NMR, water contact angle analysis, and TG/DTG measurements provide consistent and direct experimental evidence supporting the mechanistic pathway of "hydrogen-bond weakening → enhanced chain relaxation → altered thermal decomposition behavior" in CNF-III.

Revision: … Static moisture absorption tests further indicated that, in a moderate 70% humidity environment, CNF-III aerogel achieved equilibrium within 30 minutes, exhibiting an equilibrium water absorption rate of 24%, in contrast to only 5.7% for CNF-I (Supplementary Fig. 9). The substantial increase in water absorption by CNF-III suggests a significantly enhanced accessibility of its hydroxyl groups, along with a more relaxed hydrogen bond network. This observation aligns well with the FTIR analysis of hydroxyl absorption peaks, the conformational changes identified through solid-state NMR, and the accelerated dynamic water absorption behavior noted in contact angle measurements. These pieces of evidence suggest that CNF-III aerogels possess a greater number of active hydroxyl groups at the surface and exhibit higher

hydroxyl accessibility compared to CNF-I aerogels. (Manuscript, page 14-15, lines 286-296)

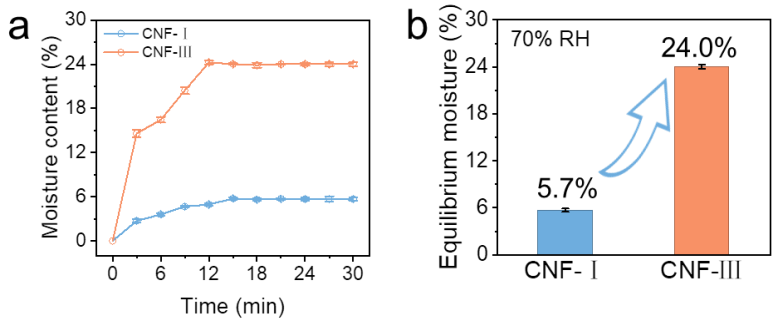

Supplementary Figure 9. Static moisture absorption test of CNF-I and CNF-III aerogels in saturated salt solution at 25 ℃ and 70% relative humidity. (**a**) Change in water content over time. (**b**) Equilibrium water content.

4. To strengthen the reliability of the conclusions related to the material's "super elasticity" or "structural robustness," it is recommended that the authors include microstructural characterization after cyclic compression.

Response: This is a very important and intuitive suggestion, as microstructural characterization after cyclic compression can directly substantiate the claimed "super elasticity" and "structural robustness" of the aerogel. In response, CNF-III@Si aerogel samples were collected immediately after completing 20,000 compression cycles and subjected to post-cycling microstructural analysis.

Scanning electron microscopy observations reveal that the aerogel retains its intact honeycomb-like porous architecture after long-term cyclic compression. No apparent cracks or collapse of the pore walls are observed, and the interconnected honeycomb network does not exhibit irreversible entanglement or fracture. In addition, the pore size

distribution shows no significant change before and after cycling, except for a slight decrease in the average pore diameter.

These results demonstrate that the three-dimensional porous framework of the aerogel remains well preserved after repeated mechanical loading, providing direct microstructural evidence for its excellent elastic recovery and structural robustness.

Revision: The microstructure and surface polymer network distribution of CNF-III@Si before and after cyclic compression exhibited negligible changes, with elements remaining uniformly distributed (Supplementary Fig. 16 and 17). This observation indicates that the structure remained intact and did not delaminate. The average pore diameter decreased by approximately 7.5 μm before and after cyclic compression, with no significant change in pore distribution, indicating that the aerogel's pore structure maintained substantial integrity (Supplementary Fig. 18). (Manuscript, page 21, lines 407-413)

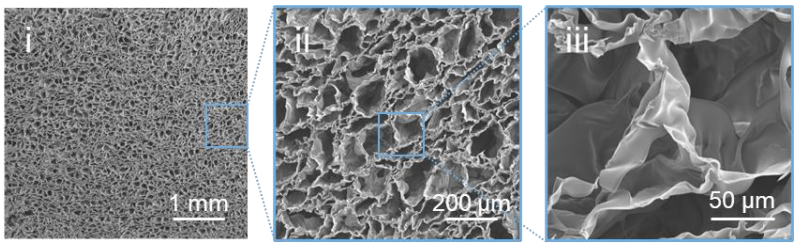

Supplementary Figure 16. SEM images of CNF-III@Si aerogel before cyclic compression.

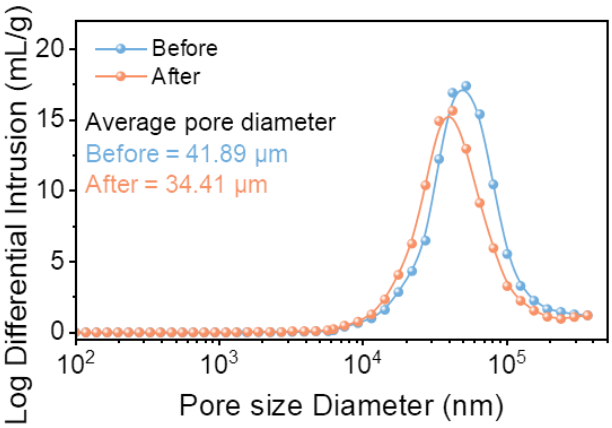

Supplementary Figure 18. Pore diameter distribution of CNF-III@Si before and after cyclic compression.

5. The current manuscript reported thermal conductivity only in a single direction; however, for cellulose-based aerogels or other porous materials, pore alignment, fiber orientation, and the distribution of the surface silanization layer may led to pronounced anisotropy in thermal conductivity. Presenting data from only one direction may not fully reflect the material's actual heat-transfer capability and makes it difficult to determine whether the topological isomerization or silanization processes alter the heat-flow pathways within the microstructure network.

Response: Thank you for this insightful and important comment. We agree that, for cellulose-based aerogels with oriented pore structures and fiber alignment, reporting thermal conductivity in only a single direction may not fully capture the actual heat-transfer behavior, nor clarify whether the topological isomerization or silanization processes modify the heat-flow pathways within the microstructural network.

In response, we have supplemented thermal conductivity measurements of the CNF-III@Si aerogel along both the direction parallel to the aligned pores (axial direction)

and the direction perpendicular to the pore alignment (radial direction). The measured axial and radial thermal conductivities are 0.0320 and 0.0328 $W \cdot m^{-1} \cdot K^{-1}$, respectively. Notably, both values are comparably low, indicating excellent thermal insulation performance in both directions.

From a microstructural perspective, axial heat transfer is influenced by the oriented pore channels formed during directional freezing. However, the extremely high porosity and the discontinuous solid framework introduce substantial interfacial thermal resistance, which suppresses the formation of efficient continuous solid-phase heat-conduction pathways. In the radial direction, although heat flow intersects more frequently with pore walls and fiber junctions, the low solid volume fraction and abundant gas–solid interfaces likewise limit effective phonon transport. As a result, heat transfer in both directions is dominated by gas-phase conduction and interfacial scattering rather than continuous solid-phase pathways, leading to comparable axial and radial thermal conductivity values.

Importantly, this near-isotropic thermal insulation behavior is advantageous for practical applications, as it reduces sensitivity to installation orientation while maintaining uniformly low thermal conductivity. The revised manuscript has been updated accordingly to clarify this point.

Revision: … Furthermore, the stable polymer topology and porous structure on the surface of the CNF-III@Si aerogel contribute to its excellent thermal insulation properties, evidenced by low thermal conductivity in both axial and radial directions at 10% relative humidity (The axial and radial thermal conductivities are 0.0320 and

0.0328 $W \cdot m^{-1} \cdot K^{-1}$ respectively. Supplementary Fig. 19). Axial heat transfer within the aerogel is affected by the directional pore channels created during the process of directional freezing. However, the extremely high porosity and discontinuous solid skeleton introduce significant interfacial thermal resistance, which inhibits the establishment of efficient heat conduction pathways. In the radial direction, although heat flow frequently intersects with pore walls and fiber connections, the low solid volume fraction and numerous gas-solid interfaces limit effective phonon transport. Therefore, bidirectional heat transfer is primarily governed by gas-phase conduction and interfacial scattering, rather than a discontinuous solid-phase thermal path, resulting in comparable axial and radial thermal conductivity values. (Manuscript, page 21-22, lines 415-429)

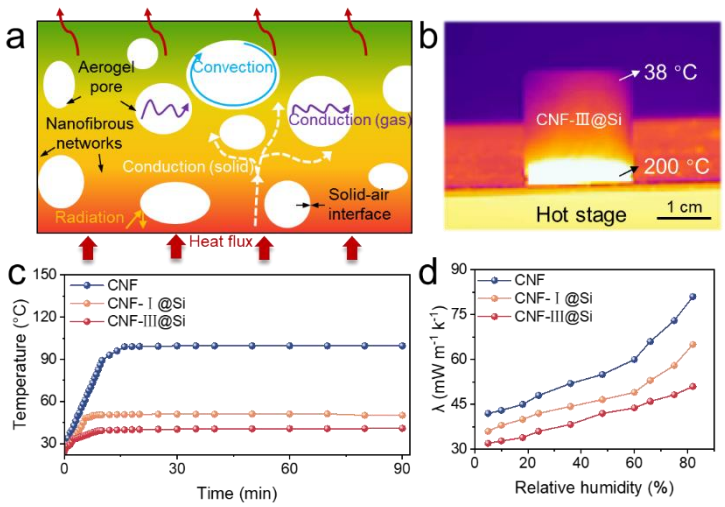

Supplementary Figure 19. The thermal insulation performance of aerogel. (**a**) Thermal insulation mechanism. Thermal conductivity is primarily composed of solid-phase conduction (λ_s), gas-phase conduction (λ_g), thermal convection (λ_c), and thermal radiation (λ_r). (**b**) The infrared thermal imaging image of CNF-III@Si aerogel on a

hotplate. (**c**) The top temperature of CNF, CNF-I@Si and CNF-III@Si aerogels changes over time. (**d**) Thermal conductivity at different relative humidities. Test results indicate that the axial and radial thermal conductivities are 0.0320 and 0.0328 $W \cdot m^{-1} \cdot K^{-1}$, respectively. These low values suggest that the material exhibits excellent thermal insulation performance in both directions. From a microstructural perspective, the axial direction provides a defined heat transfer path due to the presence of directional pore channels. However, the high porosity and discontinuous solid skeleton lead to significant interfacial thermal resistance, which impedes efficient heat conduction. In contrast, although radial heat flow interacts more frequently with the pore walls and fiber connections, the low solid content and extensive gas-solid interface also restrict phonon transmission. Consequently, bidirectional heat transfer is predominantly governed by gas phase conduction and interfacial scattering, rather than the discontinuous solid path, resulting in similar axial and radial thermal conductivities. This nearly isotropic low thermal conductivity characteristic offers advantages in practical applications, as it reduces sensitivity to installation direction while ensuring uniform thermal insulation performance.

6. It stated that CNF-III underwent more extensive silanization due to its higher hydroxyl accessibility. However, this conclusion was currently based mainly on XPS survey elemental ratios (Figure 3f) and FTIR spectra (Figure S8a) and may still lack direct experimental evidence capable of quantifying the actual reaction extent. It is recommended that the authors provide characterization methods that can quantify the Si content or the degree of silanization.

Response: Thank you for pointing out this important issue. To more rigorously and quantitatively support the conclusion that CNF-III undergoes more extensive silanization, we have supplemented the revised manuscript with inductively coupled plasma optical emission spectroscopy (ICP-OES) analysis, which allows precise determination of the absolute silicon content in the aerogels.

The ICP-OES results show that the silicon contents of CNF-I@Si and CNF-III@Si aerogels are 0.82 wt% and 1.45 wt%, respectively. Notably, the Si content in CNF-III@Si is approximately 1.76 times that of CNF-I@Si, providing direct and quantitative evidence that CNF-III experiences a more extensive silanization reaction. This enhanced degree of silanization can be reasonably attributed to the increased hydroxyl accessibility and reactivity induced by the topological isomerization process.

It should be noted that the Si atomic percentages obtained from XPS analysis in the main text (5.4 at% for CNF-I@Si and 10.5 at% for CNF-III@Si) are higher than those measured by ICP-OES. This discrepancy arises from the intrinsic differences between the two characterization techniques: XPS is a highly surface-sensitive method that probes only the near-surface region of the sample, whereas ICP-OES reflects the bulk elemental composition. Since both CNF-I@Si and CNF-III@Si aerogels were prepared via vapor-phase deposition of methyltrimethoxysilane, surface enrichment of silicon is expected, leading to higher Si contents detected by XPS compared to bulk-averaged ICP-OES results.

Taken together, the surface-sensitive XPS data and the bulk-quantitative ICP-OES results are highly consistent in trend and jointly confirm that CNF-III exhibits a higher

degree of silanization, thereby reinforcing the proposed mechanism that enhanced hydroxyl accessibility promotes more effective silane grafting.

Revision: … Inductively coupled plasma optical emission spectroscopy (ICP-OES) was used to determine the silicon content with precision. The findings revealed that the absolute silicon content in CNF-I@Si and CNF-III@Si aerogels was 0.82% and 1.45%, respectively, indicating that the latter was 1.76 times greater than the former (Supplementary Table 5). This quantitative data directly suggests that CNF-III experienced a more thorough silanization reaction. (Manuscript, page 19-20, lines 371-376)

Supplementary Table 5. Test data from an inductively coupled plasma optical emission spectrometer (ICP-OES).

Samples	m_0 (g)	V_0 (mL)	C_0 (mg/L)	f	C_1 (mg/L)	C_x (mg/kg)	W (%)
CNF-I@Si	0.0464	20	1.9153	10	19.1532	8255.69	0.8256%
CNF-III@Si	0.0485	20	3.5062	10	35.0620	14458.56	1.4459%

Calculation of Si content:

$$C_x = \frac{C_0 f V_0}{m_0} = \frac{C_1}{m_0} \quad (9)$$

$$W(\%) = \frac{C_x}{10^6} \times 100\% \quad (10)$$

where m_0 represents the sample mass, V_0 denotes the volume following digestion and final volume adjustment, f indicates the dilution factor, C_1 refers to the ratio of element concentration in the digestion solution to that in the original sample solution, C_x signifies the tested concentration, and W represents the element content in the final sample.

7. This work evaluated the triboelectric performance mainly through macroscopic output parameters such as open-circuit voltage and short-circuit current. It is recommended that the authors further quantify the surface charge density to more accurately assess how topological isomerization or silanization influences the triboelectric charging behavior of the material.

Response: We fully agree with this suggestion. To more accurately evaluate how topological isomerization and silanization influence the triboelectric charging behavior, we have supplemented the revised manuscript with quantitative measurements of surface charge density (σ), together with the corresponding output voltage and current measured at a working frequency of 2 Hz. Surface charge density provides a more intrinsic descriptor of triboelectric performance and enables a more direct comparison between CNF-I@Si and CNF-III@Si aerogels beyond macroscopic output parameters alone.

It should be noted that CNF-I@Si exhibits significantly lower compressibility than CNF-III@Si, which may partially limit its ability to achieve fully developed contact–separation cycles under identical applied pressure and nominal contact area. Since triboelectric charging is highly sensitive to the real contact area and interfacial deformation, differences in mechanical compliance can influence the measured surface charge density and output signals. To ensure the highest possible comparability, all measurements were conducted under the same applied pressure and electrode configuration. The corresponding results are included in the revised manuscript, and the potential influence of compressibility on triboelectric behavior is discussed

accordingly.

Revision: … Supplementary Fig. 23 illustrates a comparison of the triboelectric output performance between CNF-I@Si and CNF-III@Si aerogels. At 25 °C, the surface charge density, output current, and voltage of the TENG based on the CNF-III@Si aerogel surpass those of the CNF-I@Si variant. Conversely, at elevated temperatures of 200 °C, the output voltage of the CNF-I@Si aerogel-based TENG experiences a significant decline, whereas the output voltage of the CNF-III@Si aerogel-based TENG remains stable at 41.6 V. The mechanical nonlinear behavior of porous elastomer materials results in a sensing hysteresis phenomenon in the signal curve. Further testing assessed the output performance under varying compressive strengths. (Manuscript, page 25-26, lines 498-506)

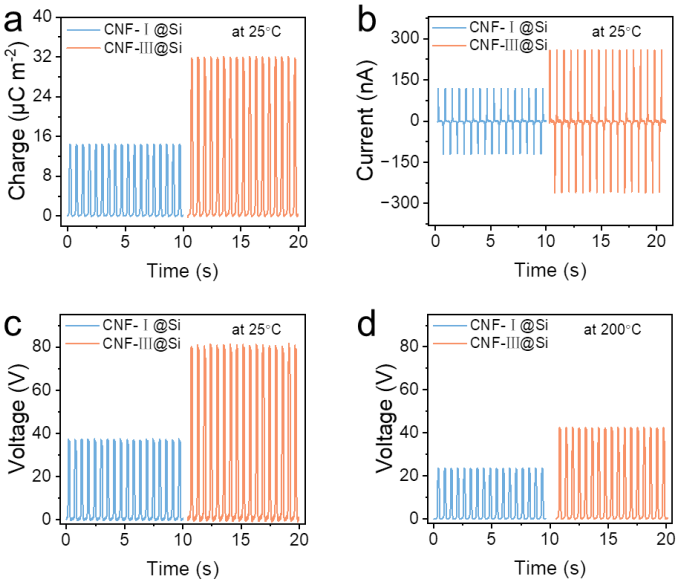

Supplementary Figure 23. Surface charge density (**a**), output current (**b**), and output voltage (**c**) of TENGs based on CNF-I@Si and CNF-III@Si aerogels at 25 °C. (**d**) Output voltage of TENGs based on CNF-I@Si and CNF-III@Si aerogels at 200 °C.

Reviewer #4 (Remarks to the Author):

The manuscript presents several noteworthy results. It demonstrates the conversion of cellulose I to cellulose III within a preformed aerogel architecture, enabling a subsequent vapor-phase siloxane crosslinking that produces an aerogel with exceptionally high elasticity, mechanical resilience, and stable triboelectric output. The combination of allomorph engineering, surface reactivity enhancement, and triboelectric performance is clearly interesting for areas including cellulose materials science, aerogel design, flexible electronics, and sensor development.

Response: We sincerely thank the reviewer for the positive and encouraging evaluation of our work. We are pleased that you recognized the core significance of this study, namely the conversion of cellulose I to cellulose III within a preformed aerogel architecture, followed by vapor-phase siloxane crosslinking enabled by enhanced surface reactivity, which together yield a cellulose aerogel combining exceptional elasticity, mechanical resilience, and stable triboelectric output.

We greatly appreciate your acknowledgment of the relevance of this integrated strategy—encompassing allomorph engineering, surface reactivity modulation, and triboelectric performance optimization—to multiple research areas, including cellulose materials science, aerogel design, flexible electronics, and sensor development. Guided by your comments, we have carefully revised the manuscript to further clarify its innovative positioning, strengthen the mechanistic discussion of structure–property relationships, and improve the overall logical rigor. We believe that the revised version more clearly and robustly conveys the unique value of this integrated design strategy.

We sincerely thank you again for your insightful comments and constructive guidance.

Overall, the data support the main conclusions, and many of the mechanical and triboelectric results are convincing. However, several aspects require clarification or deeper explanation—for example, the interpretation of hydrogen-bond distributions, the thermal degradation behavior of CNF-III, and the relationship between MD/DFT analyses and the experimental findings. These points do not invalidate the study but require revision to ensure the conclusions are fully supported.

Response: We thank the reviewer for acknowledging the overall data quality and the validity of the main conclusions. We fully agree that several aspects—namely the interpretation of hydrogen-bond distributions, the thermal degradation behavior of CNF-III, and the connection between MD/DFT analyses and experimental observations—require further clarification to ensure the rigor and completeness of the mechanistic conclusions.

We believe that these revisions significantly strengthen the mechanistic interpretation and ensure that all conclusions are fully supported. Guided by these comments, we have carefully revised the manuscript as detailed below.

(1) Interpretation of hydrogen-bond distributions.

To clarify the physical meaning of the hydrogen-bond statistics derived from MD simulations, we have added an illustrative schematic (Supplementary Fig. 4) that explicitly shows the spatial distribution of cellulose chains and the corresponding hydrogen-bond counting strategy. The MD model consists of 30 cellulose octamers

arranged in five stacked layers (six chains per layer), which reflects a commonly accepted lower bound for cellulose microfibril models. Hydrogen bonds were statistically analyzed along different crystallographic planes, allowing a more intuitive comparison between cellulose I and cellulose III. The revised discussion now more clearly links the altered hydrogen-bond network in CNF-III to increased hydroxyl accessibility.

Revision (1): … Molecular dynamics simulation (MD) was employed to investigate the impact of crystal isomerization on the accessibility of cellulose hydroxyl groups. The molecular dynamics simulation system comprises 30 octameric glucan chains organized into five layers, with six chains per layer, to construct the cellulose model (Fig. 2a, b). This arrangement is based on the consensus regarding the minimum number of molecular chains necessary to form a fundamental cellulose fiber. In comparison to CNF-I, CNF-III fibers exhibit a greater number of exposed hydroxyl groups on their surfaces. These hydroxyl groups, along with the oxygen atoms in the pyranose rings and glycosidic bonds, establish a comprehensive hydrogen bond network that includes both intramolecular and intermolecular hydrogen bonds. This hydrogen bond network is crucial for the accessibility of cellulose hydroxyl groups, ultimately influencing the modification effects and various properties of the aerogel. Fig. 2c illustrates the distinct hydrogen bond distributions of CNF-I and CNF-III (see Supplementary Fig.4 for more details). Notably, the number of intrachain hydrogen bonds per chain in the CNF-I crystal core exceeds that in CNF-III, as indicated by the corresponding 6×5 grid portion of the distribution diagram. Although the number of

intramolecular hydrogen bonds in the solvent-exposed chains is lower than that in the crystal core chains for both, the value in CNF-I remains elevated, significantly reducing its hydroxyl accessibility[16]. In terms of interchain and intra-lamellar hydrogen bonds (corresponding to the top part of the distribution diagram), CNF-III displays fewer hydrogen bonds in both the crystal core and solvent-exposed chains, which enhances the interaction between the solvent and CNF-III. Conversely, the number of inter-chain hydrogen bonds in the interlayer, corresponding to the five layered parts, shows an opposing trend. Interlayer CNF-III possesses a greater number of O3–O5 inter-chain hydrogen bonds, which are advantageous for maintaining the fiber's strength[15,43]. Numerous intramolecular O2–O6, O3–O6, and O3–O5 hydrogen bonds exist within the CNF-I sheet, where they contribute to maintaining the linear integrity and conformational rigidity of individual cellulose chains within the same fibril layer[43]. In contrast, CNF-III lacks O2–O6 intramolecular hydrogen bonds within the sheet. As a result, the C6 primary hydroxyl groups in CNF-III experience reduced intramolecular constraint, leading to increased conformational freedom and lower chain stiffness compared to CNF-I. Furthermore, the average number of inter-sheet (interlayer) hydrogen bonds between adjacent fibril layers in CNF-III exceeds that in CNF-I, which enhances interlayer cohesion and contributes to the improved mechanical strength of the aerogel. (Manuscript, page 9-10, lines 162-196)

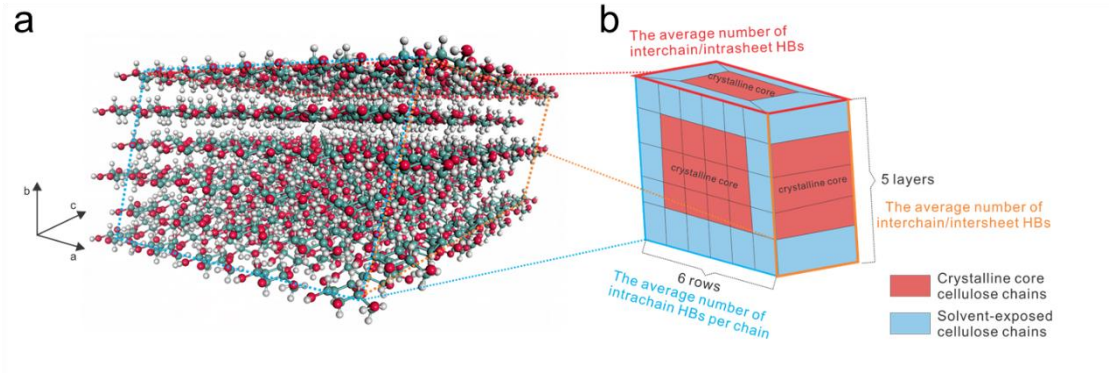

Supplementary Figure 4. (**a**) A molecular dynamics model exemplified by CNF-I. (**b**) A schematic representation illustrating the distribution of molecular chains and hydrogen bonds within cellulose crystals. Molecular chain distribution: the structure comprises five layers, each containing six octamer cellulose chains. The central chains, depicted in red, serve as the core chains, while the outer chains, shown in blue, are exposed to the solvent. Hydrogen bond distribution: the left 6×5 grid (representing the ab-plane of the crystal) indicates the average number of intra-chain hydrogen bonds per chain; the right five layers (representing the bc-plane of the crystal) illustrate the average number of hydrogen bonds between adjacent chains within each layer; the upper section displays the average number of hydrogen bonds between adjacent chains within the same layer (the ac-plane of the crystal).

(2) Thermal degradation behavior of CNF-III.

We have expanded the discussion of the TGA/DTG results and divided the thermal decomposition of CNF-III into four stages, including moisture removal, degradation associated with residual species, decomposition of crystalline domains, and final carbonization. Compared with CNF-I, CNF-III exhibits a lower residual mass after thermal decomposition, which can be attributed to its more expanded and less compact

crystalline structure, as confirmed by XRD. This behavior is consistent with previous reports (For example, Wu, Q. *et al.* The effect of surface modification on chemical and crystalline structure of the cellulose III nanocrystals. *Carbohydr. Polym.* 235, 115962 (2020); Wada, M., Kwon, G. J. & Nishiyama, Y. Structure and thermal behavior of a cellulose I-ethylenediamine complex. *Biomacromolecules* 9, 2898–2904 (2008).) on cellulose III-based materials.

Revision (2): … The TGA results indicate that the thermal degradation of CNF-III can be categorized into four distinct stages (Supplementary Fig. 7). The first stage, occurring below 100°C, involves the removal of adsorbed and bound water from the material. The second stage pertains to the thermal behavior of residual components within the aerogel, where residual amines may exert an autocatalytic degradation effect on the amorphous regions of cellulose[49]. The third stage is associated with the decomposition of cellulose crystalline components. The final stage encompasses the carbonization process of the material[50]. In comparison to CNF-I, CNF-III exhibits a lower pyrolysis char rate following thermal degradation, likely due to its more porous crystal structure, which renders it more vulnerable to damage and degradation at elevated temperatures. This finding aligns with trends documented in the existing literature[18]. TG/DTG thermal stability analysis further indicated that the CNF-III molecular chain exhibits greater flexibility than CNF-I while maintaining high stability. (Manuscript, page 12, lines 231-244)

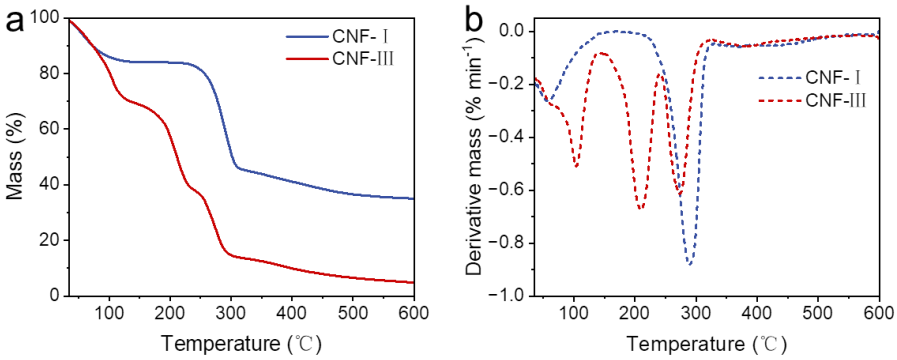

Supplementary Figure 7. TG (**a**) and DTG (**b**) curves of CNF-I and CNF-III aerogels.

The pyrolysis temperature of CNF-I is about 288 ℃, while the pyrolysis temperature of CNF-III drops to 210 ℃, indicating that the flexibility of CNF-III molecules is significantly higher than that of CNF-I. The TGA results indicate that the thermal degradation process of CNF-III can be categorized into four distinct stages. The first stage, occurring at temperatures below 100 °C, corresponds to the removal of adsorbed and bound water within the material. The second stage pertains to the thermal behavior of residual components in the aerogel, where residual amines may exert an autocatalytic degradation effect on the amorphous regions of cellulose. The third stage is associated with the decomposition of cellulose crystalline components. The final stage encompasses the carbonization process of the material. In comparison to CNF-I, CNC-III exhibits a lower pyrolysis char residue following thermal degradation, likely due to its looser crystal structure, which renders it more vulnerable to damage and degradation at elevated temperatures.

(3) Relationship between MD/DFT analyses and experimental results.

The Discussion section has been revised to explicitly bridge molecular simulations and macroscopic performance. MD simulations reveal how differences in hydrogen-

bonding patterns and conformational flexibility between cellulose I and cellulose III affect hydroxyl accessibility and subsequent functionalization efficiency. DFT calculations further demonstrate that the predominance of primary hydroxyl groups in cellulose III leads to higher HOMO energy levels and a reduced band gap, indicating enhanced chemical reactivity. These theoretical predictions are fully supported by FTIR, solid-state NMR, contact-angle measurements, and static moisture-adsorption experiments.

In addition, DFT calculations were employed to explore possible electron generation and transfer mechanisms in CNF-III@Si during triboelectric contact–separation processes. Although simplified models were used, they provide valuable insight into the electronic processes underlying the experimentally observed triboelectric behavior. Relevant discussions have been added accordingly.

Revision (3): … The transformation from cellulose I to cellulose III is accompanied by a transition from a strong, ordered hydrogen bond network to a weaker network that possesses a greater number of bonds with lower energy, which is a significant aspect of the crystalline structure of cellulose III[52]. The analysis of hydroxyl characteristic peaks in the FTIR data reflects the types and relative intensities of intramolecular and intermolecular hydrogen bonds. Additionally, molecular dynamics simulation statistics provide insights into the number and spatial distribution of hydrogen bonds. Together, these analyses confirm from different perspectives that the crystal transformation induces changes in the hydrogen bond network. (Manuscript, page 13-14, lines 267-276)

Revision (4): ... By integrating the alterations in the characteristic infrared peaks of hydroxyl groups, the chemical shift variations of C6 in solid-state NMR, the contact angle measurements, and static moisture absorption tests, we validated the molecular dynamics simulations concerning hydrogen bond distribution and conformational transitions, as well as the DFT analysis related to reactivity changes. Additionally, our findings indicate that CNF-III aerogel presents a greater number of surface-active hydroxyl groups, with enhanced accessibility compared to CNF-I aerogel. This characteristic will promote more efficient functionalization of CNF-III aerogel while preserving its high strength. (Manuscript, page 15, lines 296-304)

The work has potential significance because it combines cellulose chemistry with a siloxane topological network to overcome the classical trade-off between strength and elasticity in CNF aerogels. The reported performance exceeds many literature benchmarks. At the same time, the conversion of cellulose I to cellulose III via amine treatment is well-established, so claims of conceptual novelty or "topological isomerization" should be contextualized more carefully within the existing literature.

Response: We thank the reviewer for the insightful assessment of the potential significance of this work and for recognizing the value of integrating cellulose chemistry with a siloxane topological network to overcome the classical strength–elasticity trade-off in cellulose aerogels.

We particularly appreciate the reviewer's important comment regarding the careful contextualization of conceptual novelty. As correctly pointed out, the amine-induced

conversion of cellulose I to cellulose III is a well-established and widely reported process. In the revised manuscript, we have therefore refined and clarified the scope of the term “topological isomerization” to more accurately reflect its novelty within the existing literature. Specifically, we emphasize that the innovation of this work does not lie in the discovery of a new individual chemical transformation, but rather in the purposeful integration of a mature allomorph-engineering strategy with subsequent vapor-phase siloxane crosslinking to construct a polymer topological network within a preformed aerogel architecture.

By strengthening the discussion and comparison with prior studies, we have positioned this concept more carefully and rigorously within the current knowledge framework, thereby ensuring that the claims of novelty are focused, well-supported, and appropriately contextualized. We sincerely thank the reviewer for this critical guidance, which has greatly helped us to more precisely articulate the contribution and significance of the present study.

Revision (1): … The application of amines in the treatment of cellulose has been demonstrated to enhance its reactivity by increasing the exposure of active hydroxyl groups and reconstructing hydrogen bond networks[13–15]. For instance, amine treatment can facilitate isomerization, converting cellulose I into cellulose III, which increases the number of hydrogen bonds in the cellulose chains that are accessible to the aqueous solvent[16]. This transformation significantly improves the binding affinity of cellulose to enzymes. Although cellulose III exhibits heightened sensitivity to specific chemical treatments, there are limited reports on the further functionalization of cellulose

aerogels or amine-treated fibers[17,18]. (Manuscript, page 3, lines 47-55)

Revision (2): … Building upon previously reported mature amine-treated cellulose processes [13,16,23–25], this study utilizes the competitive hydrogen bonds formed between small-molecule EDA and cellulose to disrupt the hydrogen bond network in pre-formed cellulose I aerogels, promoting molecular chain rearrangement and driving its crystalline isomerization towards the more reactive cellulose III. Our findings indicate that this process enhances the reactivity of cellulose III without compromising the macroscopic pore structure of the aerogel. Additionally, we developed a uniform polymer topological network through in-situ polymerization and crosslinking, achieving the objective of maintaining fiber stiffness while effectively shielding inter-fiber hydrogen bonds. Following topological isomerization, the cellulose I aerogel yielded a cellulose III-based triboelectric aerogel (CNF-III@Si) that exhibits both superelasticity and high strength. Moreover, this aerogel demonstrates an ultrafast compression recovery rate and temperature-invariant elasticity, thereby creating favorable conditions for applications in extreme environments. Topological isomerization, which induces electron cloud redistribution and alters microstructure, enhances triboelectric output performance. Consequently, triboelectric nanogenerators constructed from aerogels exhibit rapid response times and highly stable outputs. Moreover, the stable output signal, sustained across a broad range of temperatures and humidity levels, underscores its significant potential for high-precision flexible sensing in extreme environments. (Manuscript, page 4-5, lines 78-97)

Revision (3): … Traditional amine treatment of cellulose powder or film materials has

been demonstrated to enhance cellulose reactivity[15,16,18,28]. Based on these findings, this study examines crystalline isomerization in the aerogel state to improve hydroxyl group accessibility and reorganize the hydrogen bond network, thereby increasing cellulose reactivity. (Manuscript, page 6, lines 110-114)

Revision (4): … The conversion of cellulose I to cellulose III through amine treatment is a well-established process. Previous studies have demonstrated that cellulose III is typically more reactive than both cellulose I and cellulose II in the preparation of cellulose derivatives[24,25]. In this study, the crystal isomerization induced by ethylenediamine treatment of CNF-I aimed to expose a greater number of active hydroxyl groups on the fiber surface, thereby facilitating chemical modification. (Manuscript, page 8-9, lines 156-161)

The experimental approach is generally sound and appropriate for the study's aims. However, several methodological descriptions lack detail for ease in reproducibility—particularly the EDA treatment and washing protocol, the MTMS vapor-phase deposition setup, triboelectric testing parameters, and aspects of the MD workflow. More details will strengthen the manuscript. I am not an expert in MD or DFT simulations, but I note that the descriptions of these methods should be made fully consistent with the detailed procedures given in the Supplementary Information.

Response: We thank the reviewer for recognizing that the overall experimental approach is sound and appropriate for the aims of this study, and for the constructive suggestions aimed at improving the clarity and reproducibility of the methodology. We

fully agree that more detailed procedural descriptions strengthen the rigor of the manuscript. In response, we have carefully revised and supplemented the *Materials and Methods* section and the Supplementary Information, as outlined below.

(1) EDA treatment and washing procedure.

In the revised manuscript, we have clarified the overall workflow of the ethylenediamine (EDA) treatment, including the sequence of processing steps, the physical state of the samples during treatment, and the subsequent washing and drying procedures. The washing process is now described more explicitly, including the washing medium, repetition strategy, and criteria used to confirm sufficient removal of residual species. A schematic illustration has been added as Supplementary Fig. 28 to improve clarity and reproducibility.

Revision (1): … CNF-III aerogel was synthesized by treating CNF I aerogel with EDA. The preparation process is illustrated in Supplementary Fig. 28. CNF I aerogel was placed in a sealed glass container with 500 mL of EDA, fully submerged using a mesh, and treated at room temperature for 12 hours. Subsequently, it was washed by immersion in 200 mL of anhydrous ethanol, and replaced with fresh ethanol at 0.5, 1.0, 2.0, 4.0, and 8 h, respectively, until the conductivity stabilized within 2 h. The aerogel was then air-dried at room temperature to a constant weight, and the resulting CNF III aerogel was sealed and stored in a desiccator for future use. The treated EDA can be recovered through vacuum distillation. (Manuscript, page 30-31, lines 582-590)

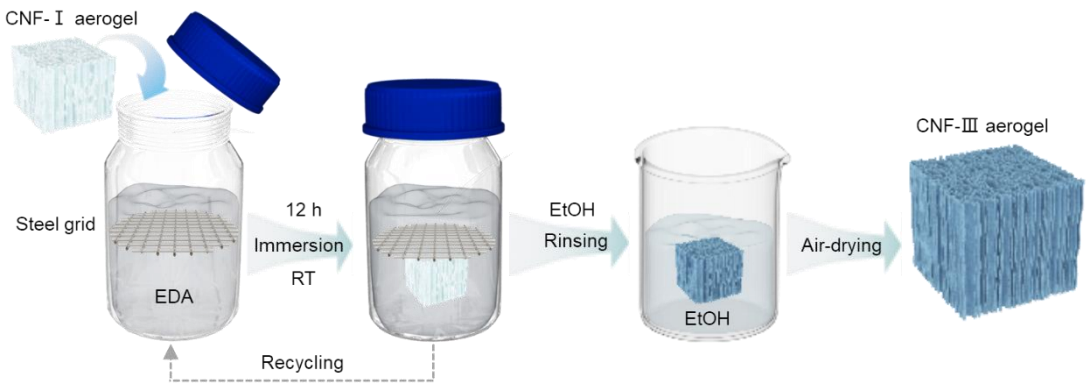

Supplementary Figure 28. The process of preparing CNF-III aerogel by EDA treatment of CNF-I aerogel.

(2) MTMS vapor-phase deposition setup.

To facilitate understanding and replication of the silanization process, we have added a schematic illustration of the MTMS vapor-phase deposition setup (Supplementary Fig. 29). The description has been expanded to more clearly explain sample placement, precursor evaporation and deposition behavior, and the overall operational procedure.

Revision (2): … The vapor-phase deposition setup is illustrated in Supplementary Fig. 29. Before the reaction, the air inside the reactor was purged three times with dry nitrogen. The aerogel was positioned within a sealed hydrothermal reactor with a volume of 350 mL. At the bottom of the reactor, two beakers were situated, one containing 1.0 mL of water and the other 1.0 mL of MTMS. The aerogel was placed on a grid, and the sealed reactor was subsequently placed in an 80 °C oven for 12 h to prepare CNF-I@Si and CNF-III@Si aerogels. (Manuscript, page 31, lines 592-598)

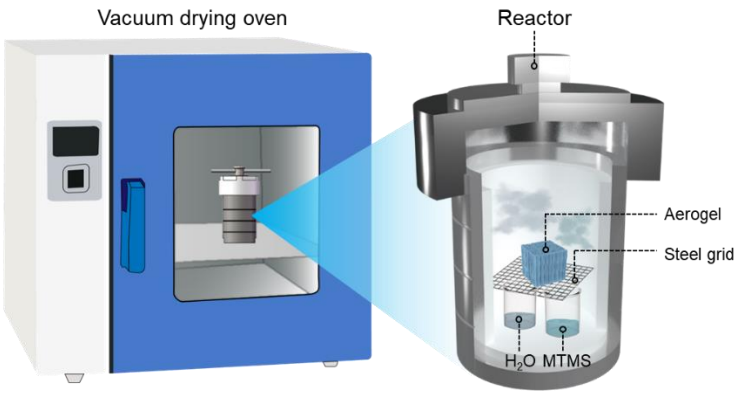

Supplementary Figure 29. Chemical vapor deposition apparatus.

(3) Triboelectric testing parameters.

The description of triboelectric measurements has been further refined by providing complete information on the testing frequency, loading mode, effective contact area, measurement environment, and data acquisition system, ensuring that the experimental conditions are clearly defined.

Revision (3): **Triboelectric output performance.** To conduct standardized measurements of electrical output, a TENG was actuated by a linear motor (LinMot E1100, Switzerland) in contact-separation mode to assess the output signal. The linear motor control unit moved a consistent distance and applied uniform pressure at a reciprocating frequency of 2.0 Hz, except when varying output signals at different frequencies was necessary. The acceleration was maintained at 1.0 m/s², with a maximum speed of 3.0 m/s, while the contact pressure was monitored using a pressure sensor (HY Chuangan HYPS017Z, China). This setup enabled precise control over the contact and separation of the two materials. The generated electrical signals were recorded by an electrometer (Keithley 6514, USA) and a data acquisition card (NI-USB6259, USA), subsequently transmitted via cable to a computer for the

measurement of open-circuit voltage, short-circuit current, and transferred charge. The final data were processed using computer software for display and recording. The test conditions for temperature and humidity were maintained at 25 °C and 65% RH, unless specific requirements dictated otherwise (different humidity or temperature).

Output signals at various frequencies were obtained by adjusting the speed of the linear motor, while maintaining constant conditions. The triboelectric nanogenerator (TENG) was secured to a heating plate using aerogel, and the output signal was recorded at different temperatures (Supplementary Fig. 30). To measure the output signal under varying humidity levels, the TENG was positioned within a custom-designed humidity-adjustable sealed chamber (Supplementary Fig. 31). (Manuscript, page 33-34, lines 643-663)

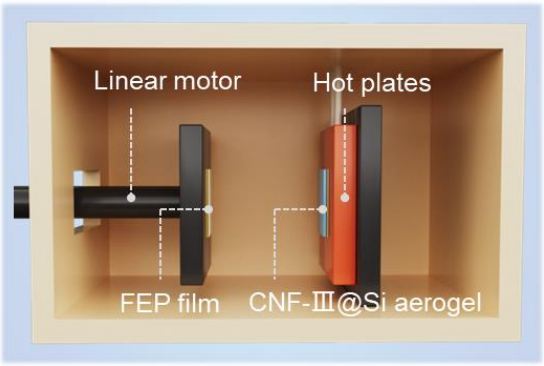

Supplementary Figure 30. High-temperature triboelectric performance testing device.

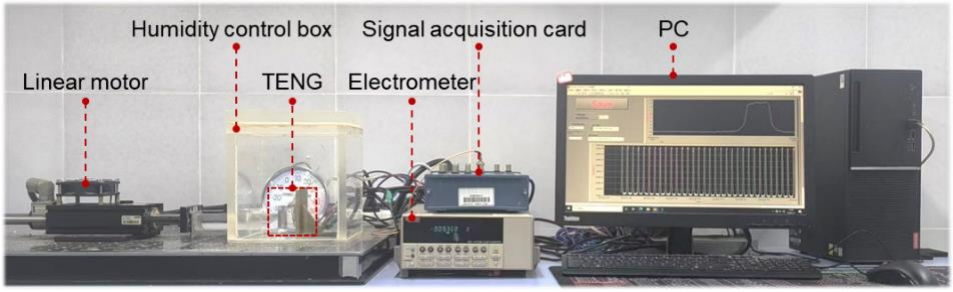

Supplementary Figure 31. Triboelectric testing device under different humidity

conditions.

(4) Consistency of the MD workflow.

In response to the reviewer's comment, we carefully cross-checked the descriptions of the MD simulation and DFT calculation in the main text and the Supplementary Information to ensure full consistency in terms of model construction, simulation workflow, and analysis methods, thereby eliminating any potential ambiguity.

We believe that these revisions significantly improve the transparency and reproducibility of the methodology. We sincerely thank the reviewer for these thoughtful and constructive comments.

Revision (4): **Molecular Dynamics Simulation.** Molecular dynamics simulations were conducted on CNF-I and CNF-III to characterize structural and dynamical features of both allomorphs. The models comprised 30 (6 × 5) octameric glucan chains for each cellulose polymorph, with crystallographic parameters obtained from literature and subsequently optimized[14,63]. Based on the consensus on the minimum limit of cellulose chains in basic cellulose fibers[14,63], 30 octamer cellulose chains were selected as a reference model. The refined parameters are documented in Supplementary Table S6, S7. All simulations utilized the CVFF force field within the LAMMPS software package under NPT conditions. Temperature and pressure were regulated by a Langevin thermostat (damping coefficient = 1.0 ps^{-1}) and a Nosé-Hoover-Langevin barostat with stochastic components (oscillation period = 200 fs, damping period = 100 fs), respectively. Nonbonded interactions employed a 10.0 Å cutoff in coordinate space, with periodic boundary conditions applied throughout.

The cellulose fibrils were immersed in a rectangular water box. To model an infinitely long fibril, each octameric cellulose chain was covalently linked to its periodic image along the fiber axis. The solvated system was first subjected to local energy minimization, followed by a short NPT-MD simulation (~0.5 ns) during which the temperature was gradually raised from 100 K to 298 K. Subsequently, a 200-ns NPT-MD production simulation was performed at 298 K and 1.01325 bar. The first 20 ns of this run were treated as equilibration, and the remaining 180 ns were used for data analysis. A timestep of 2.0 fs was used, and covalent bonds involving hydrogen atoms were constrained using the SHAKE algorithm. See the Supplementary Note 2 for more details.

Density Functional Theory Calculations. All of the density functional theory (DFT) calculations were carried out with Materials Studio DMol^3 program from Accelrys[64,65]. All initial structures were fully geometry-optimized prior to electronic structure analysis to obtain energetically stable conformations. Geometry optimizations were performed using the hybrid exchange–correlation functional B3LYP in combination with a double numerical basis set with polarization functions (DNP). The geometry optimizations were considered converged when the total energy, maximum force, and maximum displacement reached 1.0×10^{-5} Ha, 0.002 Ha Å^{-1}, and 0.005 Å, respectively. The self-consistent field convergence threshold was set to 1.0×10^{-5} Ha. It is important to note that these models may not accurately represent real reactivity or actual charge transfer processes. However, they offer valuable insights into the changes in reactivity at the molecular level and elucidate how electrons are generated and transferred in

aerogels during contact separation. See the Supplementary Note 4 for more details. (Manuscript, page 34-36, lines 664-699)

The analytical framework is mostly appropriate, but several interpretations require further justification—especially reconciling FTIR hydrogen-bond assignments with MD results, explaining early thermal degradation of CNF-III aerogels, and addressing limitations of the DFT model systems. These refinements will improve the robustness of the conclusions.

Response: We thank the reviewers for recognizing the rationality of the overall analytical framework of this work and for providing insightful and professional guidance on the explanation of key mechanisms. The three aspects you pointed out—the consistency between FTIR hydrogen bond attribution and MD results, the early thermal degradation behavior of CNF-III aerogel, and the limitations of the DFT model system—are indeed crucial to improving the logical rigor and robustness of the paper's conclusions. We fully acknowledge the importance of these issues and have addressed and strengthened them in the revised manuscript, as detailed below.

(1) Coordination between FTIR Hydrogen Bond Assignment and MD Results

To address potential gaps in understanding between FTIR and MD analyses, we systematically clarified their complementary relationship in terms of information dimensions in the revised draft.

FTIR spectra primarily reflect the strength and relative proportion changes of hydrogen bonds involved in different types of hydroxyl groups, while MD simulations provide

statistical information on the quantity, spatial distribution, and anisotropy of hydrogen bonds. By comparing the changing trends of hydroxyl absorption peaks in FTIR with the evolutionary characteristics of hydrogen bond distribution in MD, we clearly pointed out that both, from different levels but in a physically meaningful way, mutually support the core conclusion that "the transition from cellulose I to cellulose III leads to the reconstruction and overall weakening of the hydrogen bond network." The relevant statements have been further clarified and strengthened in the Results and Discussion section.

Revision (1): … The fitting of the hydroxyl characteristic peaks in FTIR analysis elucidates the distribution and intensity variations of intramolecular and intermolecular hydrogen bonds in cellulose. The fitting results indicate that CNF-I and CNF-III maintain identical compositions, as both exhibit intramolecular hydrogen bonds (O(2)H…O(6) and O(3)H…O(5)) and intermolecular hydrogen bonds (O(6)H…O(3′)). This consistency is attributed to the molecular chain stacking modes of CNF-I and CNF-III, with CNF-III preserving the parallel arrangement characteristic of CNF-I[50]. However, differences in the distribution and strength of these bonds are evident. Specifically, the proportion of weak intramolecular hydrogen bonds in CNF-III increases, with O(2)H…O(6) rising from 7.5% to 10.6%. Conversely, the proportions of strong hydrogen bond components decrease, with O(3)H…O(5) and O(6)H…O(3′) declining by approximately 2.1% and 1.0%, respectively. This alteration may result from the introduction of ethylenediamine between the cellulose molecular chains, which increases interchain spacing and diminishes the highly ordered and geometrically

constrained strong interchain hydrogen bonds in cellulose I. The O(6)H···O(3′) bond induces a degree of relaxation in the conformation of glucose units, thereby reducing the stability of the medium-strength intrachain hydrogen bonds O(3)H···O(5)[15]. The characteristic peak shifted from 3353 cm^{-1} to 3361 cm^{-1}, accompanied by a decrease in hydrogen bond energy of 4.12 kJ mol^{-1} (Supplementary Table 4), indicating a significant increase in the accessibility of hydroxyl groups[51]. Conversely, the strong intramolecular hydrogen bonds (O(3)H…O(5)) and intermolecular hydrogen bonds (O(6)H…O(3′)) in CNF-III exhibited notable blue shifts, with hydrogen bond energies decreasing by 5.59 kJ mol^{-1} and 1.73 kJ mol^{-1}, respectively (Fig. 2d, e, and Supplementary Fig. 8). The transformation from cellulose I to cellulose III is accompanied by a transition from a strong, ordered hydrogen bond network to a weaker network that possesses a greater number of bonds with lower energy, which is a significant aspect of the crystalline structure of cellulose III[52]. The analysis of hydroxyl characteristic peaks in the FTIR data reflects the types and relative intensities of intramolecular and intermolecular hydrogen bonds. Additionally, molecular dynamics simulation statistics provide insights into the number and spatial distribution of hydrogen bonds. Together, these analyses confirm from different perspectives that the crystal transformation induces changes in the hydrogen bond network. (Manuscript, page 12-14, lines 244-276)

(2) Early Thermal Degradation Behavior of CNF-III Aerogel

Regarding the issue of earlier thermal degradation of CNF-III at lower temperatures, we discussed this in more detail in the revised draft. Besides the structural relaxation

and defect factors that may be introduced by crystal configuration changes, we focused on evaluating and discussing the potential catalytic degradation effect of residual amines at low temperatures. We also supplemented the explanation of the washing steps used in sample preparation and their effectiveness verification methods, and explicitly stated in the discussion that the early thermal degradation behavior of CNF-III should be understood as the result of the combined effect of crystal structure rearrangement and trace residues, rather than being caused by a single factor. This supplement makes the explanation of the thermal behavior completer and more prudent.

Revision (2): … The TGA results indicate that the thermal degradation of CNF-III can be categorized into four distinct stages (Supplementary Fig. 7). The first stage, occurring below 100 °C, involves the removal of adsorbed and bound water from the material. The second stage pertains to the thermal behavior of residual components within the aerogel, where residual amines may exert an autocatalytic degradation effect on the amorphous regions of cellulose[48]. The third stage is associated with the decomposition of cellulose crystalline components. The final stage encompasses the carbonization process of the material[49]. In comparison to CNF-I, CNF-III exhibits a lower pyrolysis char rate following thermal degradation, likely due to its more porous crystal structure, which renders it more vulnerable to damage and degradation at elevated temperatures. (Manuscript, page 12, lines 231-244)

(3) Limitations and Scope of Application of the DFT Model System

Regarding the simplification of the DFT model system, we systematically explained the motivation, rationale, and inherent limitations of model selection in Supplementary

Note 4. For cellulose, as a polymer system, to balance computational feasibility and physical insight, we used cellulose dimers as the model unit when analyzing cellulose I and cellulose III. This structure contains β-O-4 glycosidic bonds and all the key chemical groups of the cellulose chain. Although it cannot fully represent the long-chain structure of actual CNF, its electronic structure changes can provide a key molecular-level reference for understanding reactivity differences. Similar modeling strategies have been adopted and validated in several previous studies (For example, Zhang, J. *et al.* Advanced enzyme-assembled hydrogels for the remediation of contaminated water. *Nat. Commun.* 16, 3050 (2025); Wang, Q. *et al.* Initial pyrolysis mechanism and product formation of cellulose: An Experimental and Density functional theory (DFT) study. *Sci. Rep.* 10, 3626 (2020)).

For the CNF-III@Si system, we did not rely on a single model, but instead constructed and analyzed three representative models: the ungrafted siloxane CNF-III molecular chain, a partially silane-grafted model, and a highly grafted cross-linked topological network model. This multi-model strategy aims to more closely approximate the possible coexisting molecular structures in the material. We also explicitly emphasize in the main text that these DFT results are used to reveal the relative changes in electronic structure and reaction trends, rather than to make quantitative predictions of the real system, and the scope of the relevant conclusions has been narrowed accordingly.

Revision (3): … It is important to note that these models may not accurately represent real reactivity or actual charge transfer processes. However, they offer valuable insights

into the changes in reactivity at the molecular level and elucidate how electrons are generated and transferred in aerogels during contact separation. See the Supplementary Note 4 for more details. (Manuscript, page 36, lines 695-699)

Revision (4): Cellulose is a macromolecular polymer that is linked to a glucose monomer as a basic unit that incorporates a β-O-4 glycosidic bond. To balance computational efficiency and cost, and in line with previous studies[5–7], cellobiose was selected as the computational model for the analysis of cellulose I and cellulose III. Cellobiose represents the fundamental repeating unit of cellulose and fully incorporates the characteristic β-O-4 glycosidic linkages as well as all key chemical functional groups along the cellulose molecular chains. Although this simplified model cannot fully capture the long-chain conformations of cellulose nanofibrils (CNF-I and CNF-III), its electronic structure analysis provides important molecular-level insights into the intrinsic reactivity of cellulose.

For the CNF-III@Si system, we constructed three representative models to facilitate a comprehensive analysis that aligns more closely with the material's potential structures, rather than relying on a single model. The first model features an ungrafted CNF-III chain, represented by a single fiber tetrasaccharide unit. In the second model, a -$Si(OH)_2CH_3$ group is grafted onto the fiber tetrasaccharide skeleton, denoted as CNF-III@Si-1. The third model, referred to as CNF-III@Si-2, involves siloxane grafting at all C6 sites of the tetrasaccharide unit to simulate a cross-linked polymer network structure. The simplification of these models reflects a balance between computational resource limitations and the necessity for atomic-level analysis of core interactions.

Additionally, for regular polymers such as fluorinated ethylene propylene (FEP), this study employs their periodic repeating units as the computational model, a widely accepted approach in DFT calculations for examining the electronic structure of polymers. (Supplementary Information, page 5-7)

We believe that with the aforementioned targeted supplementary explanations and revisions, the mechanistic explanations regarding hydrogen bond reconstruction, thermal degradation behavior, and theoretical calculation support in the paper will be clearer, more rigorous, and more consistent, and the robustness of the overall conclusions will be significantly enhanced. We sincerely thank you again for your insightful guidance.

The manuscript would be strengthened by clearer methodological descriptions, additional explanations for specific contradictory or unclear findings, and more cautious framing of novelty claims. These revisions are well within the scope of a typical resubmission and do not require fundamentally new experiments.

Response: We thank the reviewer for these three highly constructive and actionable suggestions, which clearly identify the key directions for strengthening the rigor, clarity, and persuasiveness of the manuscript. We fully agree with these comments and have systematically addressed them in the revised version.

First, the Materials and Methods section has been comprehensively refined and clarified, with additional details provided for experimental procedures, key parameters, and data-analysis workflows. These revisions ensure that the methodology is described in a clear,

complete, and unambiguous manner, meeting a high standard of reproducibility.

Second, we have revisited the entire manuscript to address any results that may appear contradictory or insufficiently explained. In such cases (e.g., hydrogen-bond analysis and thermal behavior), we have added more coherent mechanistic discussions and supporting evidence, thereby strengthening the logical consistency between experimental observations and their interpretation.

Finally, we have adopted a more cautious and precise framing of the novelty claims. The Introduction and Discussion have been revised to position the contribution of this work as the systematic integration of established approaches with function-oriented material design, and the conceptual significance is now more carefully contextualized through expanded literature comparisons.

We believe that these revisions substantially improve the overall quality and academic rigor of the manuscript. We sincerely thank the reviewer for their insightful and constructive evaluation.

The manuscript is generally well written and accessible. Some sections, however, would benefit from additional contextualization—e.g., the introduction includes results and the discussion is very minimal.

Response: We thank the reviewer for the positive assessment of the manuscript's writing quality and accessibility, as well as for the constructive suggestions regarding its structure. We fully agree with these comments and have made targeted revisions in the revised manuscript.

Specifically, the Introduction has been reorganized and streamlined to focus more clearly on the research background, key challenges in the field, and the objectives and overall strategy of this work. Descriptions of specific results that appeared prematurely in the original version have been removed or substantially reduced, allowing the Introduction to better serve its role in motivating the study.

Revision (1): … Building upon previously reported mature amine-treated cellulose processes[13,16,23–25], this study utilizes the competitive hydrogen bonds formed between small-molecule EDA and cellulose to disrupt the hydrogen bond network in pre-formed cellulose I aerogels, promoting molecular chain rearrangement and driving its crystalline isomerization towards the more reactive cellulose III. Our findings indicate that this process enhances the reactivity of cellulose III without compromising the macroscopic pore structure of the aerogel. Additionally, we developed a uniform polymer topological network through in-situ polymerization and crosslinking, achieving the objective of maintaining fiber stiffness while effectively shielding inter-fiber hydrogen bonds. Following topological isomerization, the cellulose I aerogel yielded a cellulose III-based triboelectric aerogel (CNF-III@Si) that exhibits both superelasticity and high strength. Moreover, this aerogel demonstrates an ultrafast compression recovery rate and temperature-invariant elasticity, thereby creating favorable conditions for applications in extreme environments. Topological isomerization, which induces electron cloud redistribution and alters microstructure, enhances triboelectric output performance. Consequently, triboelectric nanogenerators constructed from aerogels exhibit rapid response times and highly stable outputs.

Moreover, the stable output signal, sustained across a broad range of temperatures and humidity levels, underscores its significant potential for high-precision flexible sensing in extreme environments. (Manuscript, page 4-5, lines 78-97)

In addition, the Discussion section has been substantially expanded and strengthened. The revised Discussion now places the key findings in a broader literature context, provides deeper analysis of the underlying physical and chemical mechanisms, and more thoroughly addresses the implications, potential applications, and limitations of the present work. As a result, the Discussion now more fully fulfills its role in interpreting and contextualizing the results.

Revision (2): … Traditional amine treatment of cellulose powder or film materials has been demonstrated to enhance cellulose reactivity[15,16,18,28]. Based on these findings, this study examines crystalline isomerization in the aerogel state to improve hydroxyl group accessibility and reorganize the hydrogen bond network, thereby increasing cellulose reactivity. (Manuscript, page 6, lines 110-114)

Revision (3): … The conversion of cellulose I to cellulose III through amine treatment is a well-established process. Previous studies have demonstrated that cellulose III is typically more reactive than both cellulose I and cellulose II in the preparation of cellulose derivatives[24,25]. (Manuscript, page 8, lines 156-159)

Revision (4): … The elasticity of cellulose aerogels is primarily attributed to the shielding effect of hydrogen bonds among the fibers. Previous studies indicate that chemical modification using silanes or petroleum-based polymers can effectively shield

these hydrogen bonds, thereby improving elastic recovery[12,53]. In this context, uniform functionalization of the fiber surfaces is essential, as it directly influences the effectiveness of hydrogen bond shielding and ultimately impacts the material's elastic properties. (Manuscript, page 16-17, lines 316-321)

We believe that these structural revisions have improved the overall clarity and scholarly depth of the manuscript. We sincerely thank the reviewer for this thoughtful and helpful suggestion.

The manuscript cites relevant literature but should also acknowledge prior foundational work on amine-induced cellulose III formation and established cellulose surface-reactivity concepts.

Response: We thank the reviewer for this important and precise comment. We fully agree that appropriate acknowledgment of foundational work is essential for scholarly rigor and for placing the present study in its proper scientific context. We appreciate the reviewer for pointing out this aspect that required strengthening.

In the revised manuscript, we have systematically expanded and refined the relevant citations:

In the Introduction, we have added and highlighted seminal studies on amine-induced transformation of cellulose I to cellulose III, clearly stating that the amine treatment employed in this work is based on this well-established and validated chemical framework. This clarification avoids any possible overstatement of novelty regarding the cellulose allomorph conversion itself.

In the Discussion, when describing how the pretreatment enhances surface reactivity and facilitates subsequent silanization, we have incorporated representative literature on cellulose surface hydroxyl accessibility, chemical reactivity, and established modification concepts. This explicitly links our findings to broader, well-recognized principles in cellulose surface chemistry.

We believe that these additions improve the scholarly completeness of the manuscript and clarify the relationship between our work and prior foundational studies. We sincerely thank the reviewer for this constructive suggestion.

Revision (1): … The application of amines in the treatment of cellulose has been demonstrated to enhance its reactivity by increasing the exposure of active hydroxyl groups and reconstructing hydrogen bond networks[13–15]. For instance, amine treatment can facilitate isomerization, converting cellulose I into cellulose III, which increases the number of hydrogen bonds in the cellulose chains that are accessible to the aqueous solvent[16]. This transformation significantly improves the binding affinity of cellulose to enzymes. Although cellulose III exhibits heightened sensitivity to specific chemical treatments, there are limited reports on the further functionalization of cellulose aerogels or amine-treated fibers[17,18]. (Manuscript, page 3, lines 47-55)

Revision (2): … Building upon previously reported mature amine-treated cellulose processes[13,16,23–25], this study utilizes the competitive hydrogen bonds formed between small-molecule EDA and cellulose to disrupt the hydrogen bond network in pre-formed cellulose I aerogels, promoting molecular chain rearrangement and driving its crystalline isomerization towards the more reactive cellulose III. (Manuscript, page 4,

lines 78-82)

Revision (3): … Traditional amine treatment of cellulose powder or film materials has been demonstrated to enhance cellulose reactivity[15,16,18,28]. Based on these findings, this study examines crystalline isomerization in the aerogel state to improve hydroxyl group accessibility and reorganize the hydrogen bond network, thereby increasing cellulose reactivity. (Manuscript, page 6, lines 110-114)

Revision (4): The conversion of cellulose I to cellulose III through amine treatment is a well-established process. Previous studies have demonstrated that cellulose III is typically more reactive than both cellulose I and cellulose II in the preparation of cellulose derivatives[24,25]. (Manuscript, page 8, lines 156-159)

This review was prepared together with the Early Carrer Researcher Jeannie Egan following the co-review initiative. We are not experts in molecular dynamics or DFT, and our comments in these areas focus on clarity and consistency rather than technical depth.

Response: We sincerely thank the reviewer and the Early Career Researcher Dr. Jeannie Egan for their time and effort under the co-review initiative.

We fully understand and respect that the comments regarding molecular dynamics (MD) and density functional theory (DFT) focus primarily on clarity, consistency, and readability, rather than on technical depth. In the revised manuscript, we have addressed these points accordingly.

Specifically, we carefully cross-checked and unified the descriptions of MD and DFT

methods in the main text and the Supplementary Information to ensure consistent terminology, coherent explanations, and the absence of ambiguity. In addition, figure annotations and textual descriptions were streamlined and clarified so that the purpose and role of the simulations are more accessible to readers from diverse backgrounds.

We sincerely appreciate these constructive suggestions, which have significantly improved the clarity and overall readability of the manuscript.

The comments and further additions are listed in detail below:

Line 76: "CNF-III@Si" appears for the first time and should be defined in its first instance in the paper.

Response: Thank you for the reviewer's careful examination of the manuscript details. These comments are very helpful in improving the accuracy and clarity of the paper. The term "CNF-III@Si" is now explicitly defined at its first occurrence in the manuscript.

Revision: … Following topological isomerization, the cellulose I aerogel yielded a cellulose III-based triboelectric aerogel (CNF-III@Si) that exhibits both superelasticity and high strength. (Manuscript, page 5, lines 87-89)

Line 88: Paradigm feels too strong here.

Response: Thank you for pointing this out. We agree that the term *"paradigm"* may be too strong in this context and could overstate the conceptual contribution. To ensure a more cautious and accurate presentation, we have revised the wording to a more neutral expression that better reflects the scope of this work.

Revision: … The molecular chain topological isomerization strategy elucidated in this study offers innovative approaches for addressing the elastic design of bio-based materials, … (Manuscript, page 5, line 97)

Line 105: The Cell III allomorph is formed during EDA treatment, not after. This is presented misleading. Enter a "has": … the crystal from has transitioned. Further, "guest" feels like a weird word. Better use something like "tempoararily bonded".

Response: Thank you for this careful and helpful comment regarding the wording and temporal description. We recognized that the original text could be misleading with respect to the timing of the cellulose I to cellulose III transformation. Following your suggestion, we have revised the manuscript to clearly state that the crystal transition occurs during the EDA treatment, while the resulting cellulose III structure is retained after removal of the temporarily bonded EDA. The text has been updated accordingly to eliminate any potential ambiguity.

Revision: … During EDA treatment, the crystal form transitions from cellulose I to cellulose III (CNF-III), which is retained after removal of the temporarily bonded EDA (Fig. 1a). (Manuscript, page 6, lines 116-118)

Line 124: "topoisomerization". We suggest to keep the language consistent: topological isomerization.

Response: Thank you for pointing out this inconsistency. We have carefully revised the manuscript and standardized the terminology to "topological isomerization" throughout the text to ensure consistency and clarity.

Figure 1d: there are several misspellings in the image: Carbon mocrolattices --> microlattices; Cubic raphene aerogels --> cubic graphene aerogels; Elastic but week --> elastic but weak; Yong's modulus --> Young's modulus

Response: We sincerely thank the reviewer for the careful proofreading of the figure. All spelling errors in Fig. 1d have been corrected.

Figure 1e: also a small misspelling: TEGN --> TENG (for triboelectric nanogenerator)

Response: Thank you for pointing out the misspelling in Figure 1e. The term "TEGN" has been corrected to "TENG".

Line 145: The O2-O6, O3-O6 hydrogen bonds are intramolecular bonds that stiffen the cellulose chain and the O3-O5 hydrogen bond is intermolecular between the cellulose chains. The authors may want to work that out in the text to the reader for a better understanding why the O2-O6 reduces stiffness.

e.g. Credou, J. and T. Berthelot, Cellulose: from biocompatible to bioactive material. Journal of Materials Chemistry B, 2014. 2(30): p. 4767-4788.

Response: We sincerely thank the reviewer for this insightful and technically important comment, as well as for pointing us to the relevant foundational literature. We agree that a clearer distinction between different types of hydrogen bonds is essential for helping readers understand why changes in specific hydrogen bonds influence cellulose chain stiffness.

As discussed in the cited work by Credou and Berthelot (*Journal of Materials*

Chemistry B, 2014. 2(30): p. 4767-4788), cellulose possesses an extensive hydrogen-bonding network comprising both intra- and intermolecular hydrogen bonds. Intramolecular hydrogen bonds, such as O3H–O5 and O2H–O6, are primarily responsible for maintaining the linear integrity and conformational rigidity of individual cellulose chains, whereas intermolecular hydrogen bonds govern chain packing, crystallinity, and supramolecular organization. The O3H–O5 hydrogen bond is the most prevalent intramolecular interaction and is shared by nearly all cellulose allomorphs, playing a key role in stabilizing the linear chain conformation. In contrast, O2H–O6 hydrogen bonds occur only in certain allomorphs and are more sensitive to structural rearrangement.

In our study, the pronounced reduction of O2–O6 intramolecular hydrogen bonds in CNF-III does not indicate strengthened interchain interactions. Rather, it reflects a release of intramolecular constraints that previously restricted the rotational freedom of the C6 group. The weakening of O2–O6 hydrogen bonding increases the conformational flexibility and accessibility of C6 hydroxyls, thereby reducing the intrinsic stiffness of the cellulose chain and facilitating local chain relaxation. This mechanism directly explains why a decrease in O2–O6 hydrogen bonding leads to reduced chain rigidity and enhanced hydroxyl reactivity.

We have revised the manuscript accordingly to explicitly distinguish the structural roles of O2–O6 and O3–O5 hydrogen bonds and to clarify the mechanistic link between reduced O2–O6 intramolecular hydrogen bonding and decreased chain stiffness.

Revision: … Numerous intramolecular O2–O6, O3–O6, and O3–O5 hydrogen bonds

exist within the CNF-I sheet, where they contribute to maintaining the linear integrity and conformational rigidity of individual cellulose chains within the same fibril layer. In contrast, CNF-III lacks O2–O6 intramolecular hydrogen bonds within the sheet. As a result, the C6 primary hydroxyl groups in CNF-III experience reduced intramolecular constraint, leading to increased conformational freedom and lower chain stiffness compared to CNF-I. Furthermore, the average number of inter-sheet (interlayer) hydrogen bonds between adjacent fibril layers in CNF-III exceeds that in CNF-I, which enhances interlayer cohesion and contributes to the improved mechanical strength of the aerogel. (Manuscript, page 10, lines 187-196)

This sounds understandable and expectable to me, but on the other hand you write:

Line 179: Figure 2d and Table S3 report an increase of O2-O6 hydrogen bonds from 7.5 to 10.6% and a reduction of the other two in an approximate ratio of 2:1 (B:C). Please provide an explanation for this finding and how it fits with the simulation data.

Response: Thank you for this thoughtful observation. The apparent change in the relative proportions of hydrogen-bond types arises from the different but complementary information provided by FTIR analysis and MD simulations.

The FTIR spectra were deconvoluted in the O–H stretching region to extract peak positions and relative intensities associated with hydroxyl groups at different locations. Based on established assignments reported in the literature (*ACS Sustain. Chem. Eng*. 2023. 11(4): p. 1581-1590; *Renew Energy*. 2015. 80: p. 132-139), the relative contributions of O2–O6, O3–O5, and O6–O3′ hydrogen bonds were estimated from the

fitted components. In contrast, the MD simulations directly quantify the number and spatial distribution of hydrogen bonds within the modeled crystalline domains, including intramolecular bonds, intralayer intermolecular bonds, and interlayer interactions. Thus, FTIR reflects the type and relative strength of hydrogen bonds, whereas MD provides their population and spatial organization. Together, they offer complementary perspectives on hydrogen-bond reconstruction during the cellulose I → cellulose III transition.

As shown in Fig. 2d and Supplementary Table 4 (formerly Table S3), the fraction of the weaker O2H···O6 hydrogen bonds increases from 7.5% to 10.6% upon conversion from cellulose I to cellulose III, while the stronger O3H···O5 and O6H···O3′ components decrease in an approximate 2:1 ratio. This trend is consistent with the relative hydrogen-bond strengths (O2H···O6 < O3H···O5 < O6H···O3′) and agrees well with the overall tendency observed in the MD simulations.

Specifically, the formation of cellulose III involves lattice relaxation and molecular chain rearrangement, which increase the conformational freedom of the hydroxymethyl group. The partial transition of the C6 hydroxymethyl conformation from *tg* to the more flexible *gt* state reduces geometric constraints and favors the formation of O2H···O6 hydrogen bonds. Consequently, the relative contribution of weaker hydrogen bonds increases. At the same time, the ethylenediamine-induced transformation disrupts the highly ordered strong intermolecular hydrogen-bond network in cellulose I, leading to a reduction in the O6H···O3′ and O3H···O5 hydrogen bonds. This redistribution reflects an evolution from a rigid, strong hydrogen-bond network toward a more

flexible and dynamic one, which is fully consistent with the hydrogen-bond population and conformational flexibility obtained from the MD simulations.

We have clarified this interpretation in the main text and in Supplementary Note 5 by explicitly introducing the concept of "hydrogen-bond network reconstruction" and by integrating the compositional FTIR analysis (Fig. 2d) with the MD-derived dynamical data.

Revision: … The fitting of the hydroxyl characteristic peaks in FTIR analysis elucidates the distribution and intensity variations of intramolecular and intermolecular hydrogen bonds in cellulose. The fitting results indicate that CNF-I and CNF-III maintain identical compositions, as both exhibit intramolecular hydrogen bonds (O(2)H…O(6) and O(3)H…O(5)) and intermolecular hydrogen bonds (O(6)H…O(3′)). This consistency is attributed to the molecular chain stacking modes of CNF-I and CNF-III, with CNF-III preserving the parallel arrangement characteristic of CNF-I[50]. However, differences in the distribution and strength of these bonds are evident. Specifically, the proportion of weak intramolecular hydrogen bonds in CNF-III increases, with O(2)H…O(6) rising from 7.5% to 10.6%. Conversely, the proportions of strong hydrogen bond components decrease, with O(3)H…O(5) and O(6)H…O(3′) declining by approximately 2.1% and 1.0%, respectively. This alteration may result from the introduction of ethylenediamine between the cellulose molecular chains, which increases interchain spacing and diminishes the highly ordered and geometrically constrained strong interchain hydrogen bonds in cellulose I. The O(6)H···O(3′) bond induces a degree of relaxation in the conformation of glucose units, thereby reducing

the stability of the medium-strength intrachain hydrogen bonds O(3)H···O(5)[15]. The characteristic peak shifted from 3353 cm^{-1} to 3361 cm^{-1}, accompanied by a decrease in hydrogen bond energy of 4.12 kJ mol^{-1} (Supplementary Table 4), indicating a significant increase in the accessibility of hydroxyl groups[51]. Conversely, the strong intramolecular hydrogen bonds (O(3)H…O(5)) and intermolecular hydrogen bonds (O(6)H…O(3′)) in CNF-III exhibited notable blue shifts, with hydrogen bond energies decreasing by 5.59 kJ mol^{-1} and 1.73 kJ mol^{-1}, respectively (Fig. 2d, e, and Supplementary Fig. 8). The transformation from cellulose I to cellulose III is accompanied by a transition from a strong, ordered hydrogen bond network to a weaker network that possesses a greater number of bonds with lower energy, which is a significant aspect of the crystalline structure of cellulose III[52]. The analysis of hydroxyl characteristic peaks in the FTIR data reflects the types and relative intensities of intramolecular and intermolecular hydrogen bonds. Additionally, molecular dynamics simulation statistics provide insights into the number and spatial distribution of hydrogen bonds. Together, these analyses confirm from different perspectives that the crystal transformation induces changes in the hydrogen bond network. (Manuscript, page 12-14, lines 243-276)

Line 176: Figure 5 shows that below 150 °C there is a lot of crystal water in Cell-I and much more in Cell-III. Thermal degradation in Cell-III seems to start before 200 °C. Please explain. Is that because of remaining residues, e.g. of ethanolamine? Ammonia may cause autocatalytic degradation.

Response: We thank the reviewer for this careful and important question. We agree that under practical experimental conditions, ethylenediamine (EDA) is difficult to remove completely, and trace residues may remain in CNF-III. However, based on a combination of thermal analysis and structural considerations, we believe that the larger mass loss below 150 °C and the earlier onset of thermal degradation in CNF-III are primarily governed by changes in the hydrogen-bonding network and water state induced by the cellulose I → cellulose III transformation, with residual EDA playing a secondary, facilitating role.

During the EDA-induced conversion from cellulose I to cellulose III, part of the strong intermolecular hydrogen-bond network is disrupted, leading to an increased interchain spacing and a more relaxed crystal lattice. This structural relaxation significantly enhances the accessibility of hydroxyl groups and the affinity of the material toward water molecules, allowing water to be retained more readily as crystalline water or strongly bound water in CNF-III. As a result, CNF-III exhibits a more pronounced mass loss below 150 °C. Supporting this interpretation, we have added static moisture-uptake measurements showing that, under identical conditions, the water absorption of CNF-III is nearly four times that of CNF-I.

At the same time, the reduction in strong intermolecular hydrogen bonds weakens the cooperative stabilization between cellulose chains, thereby lowering the energetic barrier for dehydration and glycosidic bond cleavage. This provides a structural explanation for the earlier onset of thermal degradation of CNF-III, which begins at around 200 °C.

We acknowledge that the potential influence of residual EDA cannot be completely excluded. The presence of amine groups may slightly promote low-temperature dehydration or the initial degradation process through weak basicity or hydrogen-bond competition. Nevertheless, considering the limited residual amount and the fact that the main mass-loss region in the thermogravimetric curves still corresponds to the characteristic degradation temperature range of the cellulose backbone, we conclude that residual EDA is not the dominant factor responsible for the reduced thermal stability of CNF-III. Instead, the observed behavior arises from the combined effects of hydrogen-bond reconstruction and altered water states associated with the cellulose III crystal structure. Similar thermal behavior of cellulose III has also been reported in previous studies (e.g., Wada et al., Structure and thermal behavior of a cellulose I-ethylenediamine complex. *Biomacromolecule*, 2008. 9: p. 2898–2904. Wu, Q. *et al.* The effect of surface modification on chemical and crystalline structure of the cellulose III nanocrystals. *Carbohydr. Polym.* 2020. 235: p. 115962.), further supporting this interpretation.

In the revised manuscript, we have added a dedicated discussion to clarify the thermal decomposition behavior of CNF-III in light of these factors.

Revision: … The TGA results indicate that the thermal degradation of CNF-III can be categorized into four distinct stages (Supplementary Fig. 7). The first stage, occurring below 100 °C, involves the removal of adsorbed and bound water from the material. The second stage pertains to the thermal behavior of residual components within the aerogel, where residual amines may exert an autocatalytic degradation effect on the

amorphous regions of cellulose[48]. The third stage is associated with the decomposition of cellulose crystalline components. The final stage encompasses the carbonization process of the material[49]. In comparison to CNF-I, CNF-III exhibits a lower pyrolysis char rate following thermal degradation, likely due to its more porous crystal structure, which renders it more vulnerable to damage and degradation at elevated temperatures. This finding aligns with trends documented in the existing literature[18]. TG/DTG thermal stability analysis further indicated that the CNF-III molecular chain exhibits greater flexibility than CNF-I while maintaining high stability. (Manuscript, page 12, lines 231-244)

Since the thermal conductivity experiments were performed at 200 °C. How do these results fit together? TGA of Silica-containing gels are not presented. Please explain. Discuss if the washing process was sufficient to remove the solvent and if incomplete removal contributes to the observed TGA effect.

Response: We sincerely thank the reviewer for raising this important question regarding the thermal conductivity measurements, TGA results, and the potential influence of residual solvent. We provide the following clarifications:

Thermal conductivity measurements at 200 °C: The measurement temperature was selected to reflect practical operating conditions, and the samples were held at a constant temperature rather than continuously heated. The thermal conductivity obtained at 200 °C therefore reflects heat transport under conditions where the material's structure remains essentially intact, rather than being dominated by thermal

degradation. In this sense, the thermal conductivity and TGA results probe complementary aspects of the material's thermal behavior.

TGA of CNF-III@Si samples: We agree that the thermal stability of silica-containing aerogels is critical for interpreting the results. In the revised manuscript, TGA data for CNF-III@Si have been added (Supplementary Fig. 20). The results show that incorporation of the siloxane topological network significantly enhances the thermal stability of the cellulose backbone. The Si–O covalent network restricts polymer chain motion and provides interfacial thermal shielding, leading to higher decomposition onset and maximum weight-loss temperatures, as well as increased char residue at high temperature. This confirms that the topological network improves both mechanical properties and thermal stability, enabling the aerogel to maintain its structure over a wider temperature range.

Influence of washing and residual solvent: We acknowledge that in highly porous and hydrophilic structures, small molecules such as ethanolamine may be difficult to remove completely and can remain via hydrogen bonding or adsorption. Such residuals can contribute to low-temperature weight loss in TGA, as observed in CNF-III, and similar phenomena have been reported in the literature (e.g., Wada et al., Structure and thermal behavior of a cellulose I-ethylenediamine complex. *Biomacromolecule*, 2008. 9: p. 2898–2904). However, the effect is minor compared to the structural contributions: the cellulose chains and silica network dominate the high-temperature thermal behavior, especially in CNF-III@Si.

In summary, the thermal conductivity measurements at 200 °C reflect the intrinsic heat

transport of the intact structure, while TGA provides complementary insight into decomposition. The washing process is largely effective, and any residual solvent contributes only modestly to early weight loss without compromising the validity of the thermal conductivity data.

Revision: … Thermogravimetric analysis (TGA) indicates that the thermal degradation temperature of CNF-III@Si reaches 290 °C (Supplementary Fig. 20). This enhanced thermal stability arises from the cross-linking of hydroxyl groups on the cellulose surface with the topological polymer network, which forms stable Si–O–C and Si–O–Si networks on the pore walls. The high bond energy and excellent thermal stability of the Si–O bonds effectively suppress chain breakage and volatilization during heating. Furthermore, the Si-O network serves as a protective barrier, impeding heat and mass transfer while promoting the formation of a silicon-rich carbon layer at elevated temperatures. This process further delays thermal degradation and contributes to the improved char yield observed in the TGA results. (Manuscript, page 22, lines 429-438)

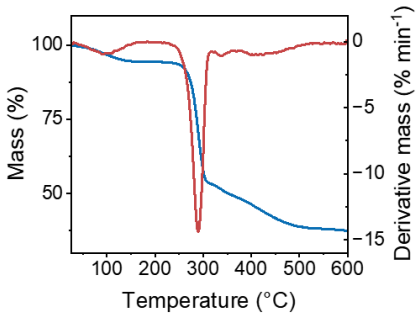

Supplementary Figure 20. TG and DTG curves of CNF-III@Si aerogel.

Line 191: I recommend adding “at the surface”: “…possess a greater number of active hydroxyl groups at the surface and…”

Response: It has been added. The revised sentence is as follow:

Revision: …possess a greater number of active hydroxyl groups at the surface and... (Manuscript, page 15, line 295)

Line 262: "…. Minimal plastic deformation." I agree that the properties are superior to the comparative materials, however I can recognize a reduction of about 40% in Fig. 4d. Is that correct?

Response: We thank the reviewer for pointing out this important detail. We agree that, as shown in Fig. 4d, the compressive strength of the aerogel decreases by approximately 40% after ~20,000 compression cycles, reflecting gradual mechanical fatigue under long-term cyclic loading.

It should be clarified that the statement "minimal plastic deformation" refers primarily to the macroscopic geometric recovery of the material. During cyclic compression, the aerogel's height reduces by only ~5% after unloading, indicating good shape recovery and negligible irreversible deformation at the macroscopic level. From a mechanical perspective, this is generally considered a sign of low plastic deformation.

Meanwhile, the decrease in compressive strength mainly arises from microscale structural damage, such as local fiber bending, node rearrangement, or gradual interface fatigue, rather than overall structural collapse. Thus, mechanical degradation does not equate directly to plastic deformation and can occur even when macroscopic deformation is small.

Based on the reviewer's suggestion, we have clarified the text in the revised manuscript,

specifying that “minimal plastic deformation” refers to limited irreversible macroscopic geometric change, avoiding confusion with the observed reduction in compressive strength.

Revision: … After 20,000 cycles of compression at 50% strain, the maximum strength of CNF-III@Si aerogel was maintained at 108.5 kPa, with its geometric height and shape remaining nearly unchanged (Fig. 4d). The observed decrease in strength is likely attributable to the accumulation of damage at the microstructural level, including skeletal bending, node rearrangement, or progressive interface fatigue, rather than an overall structural collapse. (Manuscript, page 20, lines 395-401)

Line 317: Delete “characteristic”.

Response: It has been corrected.

Line 327: The output signal changed less than 0.5% correct?. If yes, remove “rate”.

Response: We appreciate your careful attention to the wording. After verification, the output signal indeed changed by less than 0.5%. Following your suggestion, we have removed “rate” and revised the sentence.

Revision: … After 12,000 cycles, the output signal change was less than 0.5%, which is adequate for the application requirements of most daily human activities (Supplementary Fig. 25). (Manuscript, page 27, lines 518-520)

The description of materials and methods is sometimes vague and lacks details:

Line 366 ff: Did the volume change after freeze drying. If yes, how much? Were the

gels stored in the desiccator afterwards?

Response: We thank the reviewer for this valuable comment. After freeze-drying, the aerogels experienced a slight volume shrinkage; we have added the following clarification in the manuscript:

Revision: … The volume of the freeze-dried aerogel is approximately 99.5% of that of the original wet gel, primarily attributable to radial shrinkage, which measures approximately 1.995 × 1.995 × 2 cm^3. Given the strong hydrophilicity of CNF-III, all dried samples were stored in a desiccator to prevent re-humidification. (Manuscript, page 30, lines 576-580)

Line 373 ff: How often was the rinsing process performed. How did you decide on the rinsing process? This is relevant in view of potential incomplete removal of the solvent.

Response: We appreciate the reviewer's attention to this detail. We have provided a more detailed description of the rinsing procedure in the revised manuscript. The number of rinsing cycles was determined based on monitoring the conductivity of the washings, ensuring that the solvent was effectively removed. To more clearly illustrate the preparation process, we have also added Supplementary Fig. 28.

Revision: CNF-III aerogel was synthesized by treating CNF I aerogel with EDA. The preparation process is illustrated in Supplementary Fig. 28. CNF I aerogel was placed in a sealed glass container with 500 mL of EDA, fully submerged using a mesh, and treated at room temperature for 12 hours. Subsequently, it was washed by immersion in 200 mL of anhydrous ethanol, and replaced with fresh ethanol at 0.5, 1.0, 2.0, 4.0, and

8 h, respectively, until the conductivity stabilized within 2 h. The aerogel was then air-dried at room temperature to a constant weight, and the resulting CNF III aerogel was sealed and stored in a desiccator for future use. The treated EDA can be recovered through vacuum distillation. (Manuscript, page 30-31, lines 582-590)

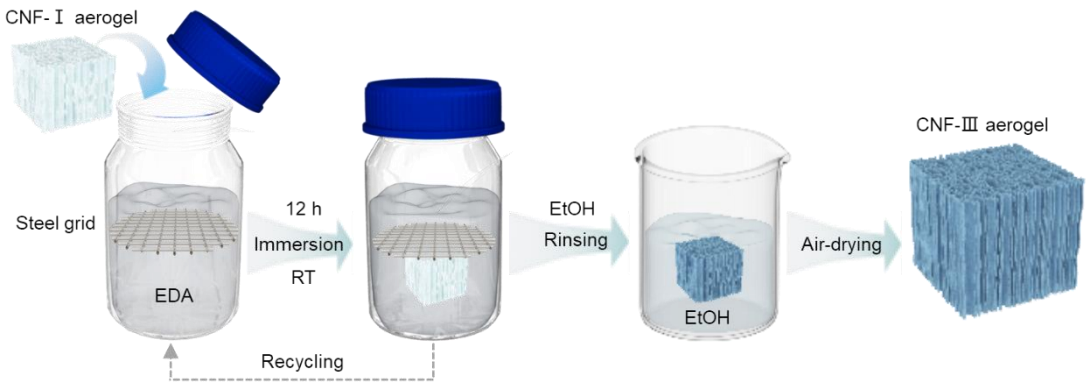

Supplementary Figure 28. The process of preparing CNF-III aerogel by EDA treatment of CNF-I aerogel.

Line 379 ff: Please provide the reactor volume and if the reactor was purged with an inert gas. Did you use deionized water?

Response: We thank the reviewer for this suggestion. In the revised manuscript, we have provided additional details of the reactor, including its volume and the use of deionized water for the chemical vapor deposition. To more clearly illustrate the preparation process, we have also added Supplementary Fig. 29.

Revision: The vapor-phase deposition setup is illustrated in Supplementary Fig. 29. Before the reaction, the air inside the reactor was purged three times with dry nitrogen. The aerogel was positioned within a sealed hydrothermal reactor with a volume of 350 mL. At the bottom of the reactor, two beakers were situated, one containing 1.0 mL of

deionized water and the other 1.0 mL of MTMS. The aerogel was placed on a grid, and the sealed reactor was subsequently placed in an 80 °C oven for 12 h to prepare CNF-I@Si and CNF-III@Si aerogels. (Manuscript, page 31, lines 592-598)

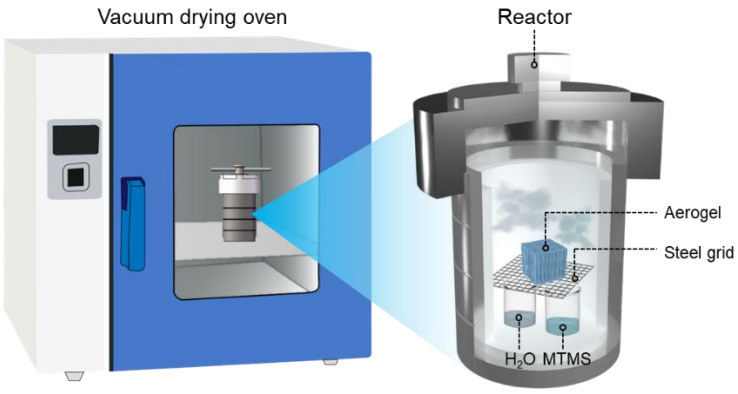

Supplementary Figure 29. Chemical vapor deposition apparatus.

Line 392: Was TGA performed in air or nitrogen? I suppose nitrogen atmosphere since in S5 you write pyrolysis.

Response: We thank the reviewer for the careful scrutiny of the experimental conditions. Your assumption is correct—TGA was performed under a nitrogen atmosphere, and this information has now been explicitly added to the manuscript.

Revision: … The thermogravimetric analysis (TGA) was performed using a thermogravimetric analyzer (TGA 8000 Perkin Elmer, USA) under a 100 mL/min nitrogen flow with a temperature ramp from 25 to 600 °C at 10 °C/min. (Manuscript, page 31, lines 612-615)

Line 411ff: More details needed. Voltage, cycles per second (2 per second?).

Response: We thank the reviewer for the comment. We have now provided a more

detailed description of the triboelectric testing procedure in the manuscript, including the applied voltage and testing frequency. In addition, to more clearly illustrate the testing process, we have added the procedures for measurements under different temperature and humidity conditions.

Revision: **Triboelectric output performance.** To conduct standardized measurements of electrical output, a TENG was actuated by a linear motor (LinMot E1100, Switzerland) in contact-separation mode to assess the output signal. The linear motor control unit moved a consistent distance and applied uniform pressure at a reciprocating frequency of 2.0 Hz, except when varying output signals at different frequencies was necessary. The acceleration was maintained at 1.0 m/s^2, with a maximum speed of 3.0 m/s, while the contact pressure was monitored using a pressure sensor (HY Chuangan HYPS017Z, China). This setup enabled precise control over the contact and separation of the two materials. The generated electrical signals were recorded by an electrometer (Keithley 6514, USA) and a data acquisition card (NI-USB6259, USA), subsequently transmitted via cable to a computer for the measurement of open-circuit voltage, short-circuit current, and transferred charge. The final data were processed using computer software for display and recording. The test conditions for temperature and humidity were maintained at 25 °C and 65% RH, unless specific requirements dictated otherwise (different humidity or temperature).

Output signals at various frequencies were obtained by adjusting the speed of the linear motor, while maintaining constant conditions. The triboelectric nanogenerator (TENG) was secured to a heating plate using aerogel, and the output signal was recorded at

different temperatures (Supplementary Fig. 30). To measure the output signal under varying humidity levels, the TENG was positioned within a custom-designed humidity-adjustable sealed chamber (Supplementary Fig. 31). (Manuscript, page 33-34, lines 643-663)

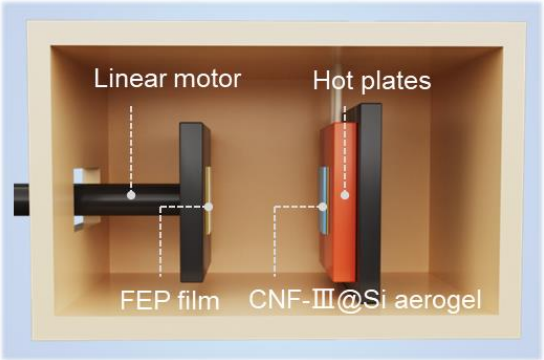

Supplementary Figure 30. High-temperature triboelectric performance testing device.

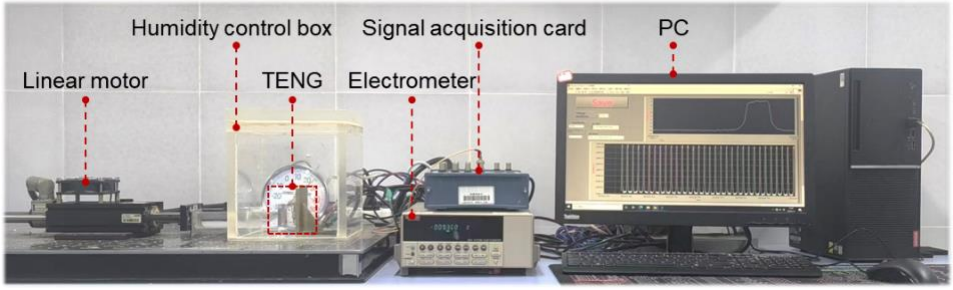

Supplementary Figure 31. Triboelectric testing device under different humidity conditions.

Supplement:

Supplementary Note 2: Molecular Dynamics Simulation details:

Last section, torsion angles: check the order of the mentioned tables. Should it be Tables S1 and S2 instead of Tables S3 and S4, as mentioned in the manuscript line 155?

Response: We sincerely thank the reviewer for carefully checking the Supplementary

Information and pointing out this inconsistency. You are correct: in the original manuscript, the references in line 155 should be to Tables S1 and S2 (molecular dynamics statistics, now Supplementary Tables 2 and 3), while those mentioned in Supplementary Note 2 should refer to Tables S3 and S4 (MD-simulated crystal unit cell parameters, now Supplementary Tables 6 and 7).

Figure S9: The caption is not correct. There should be a and b instead of c and d.

Response: The caption has been corrected.

Figure S11 is lacking the “S”.

Response: We appreciate your careful attention to the figure labeling. In accordance with the journal’s formatting requirements, the figure label has been updated. For example, “Figure S11” has been corrected to “Supplementary Figure 11.”

Additionally, I would like to mention:

The paper introduces this as a new concept, but the underlying chemistry (Cellulose I → Cellulose III via amines) is well-known. Please contrast the definition with traditional cellulose polymorph conversion. Clarify what is topological beyond crystallographic rearrangement and remove novelty overstatements.

Response: We appreciate this important and insightful comment. We fully agree that the chemical conversion of cellulose I to cellulose III via amines is well-established in the literature. The novelty of our work does not lie in this basic chemical transformation but in the introduction and elucidation of the concept of topological isomerization of

cellulose aerogels and its structural-functional implications.

In the revised manuscript, we clarify and contrast as follows:

Traditional cellulose polymorph conversion mainly involves chain rearrangements within the crystal lattice (e.g., cellulose I → III) and often disrupts the macroscopic fiber morphology.

Our "topological isomerization of cellulose aerogels" emphasizes that during the polymorphic transition, the original 3D network architecture, high aspect ratio, and continuous fiber morphology of the nanofibers are preserved, maintaining the aerogel's pores, walls, and honeycomb structures. This represents inheritance and remodeling at the mesoscale structural level.

We have carefully revised the Introduction, Result and Discussion to avoid overstatement of novelty regarding the chemical pathway itself, instead highlighting the innovation in achieving controlled topological inheritance and functional enhancement of cellulose nanofibers via a known chemical route.

Revision (1): … The application of amines in the treatment of cellulose has been demonstrated to enhance its reactivity by increasing the exposure of active hydroxyl groups and reconstructing hydrogen bond networks[13–15]. For instance, amine treatment can facilitate isomerization, converting cellulose I into cellulose III, which increases the number of hydrogen bonds in the cellulose chains that are accessible to the aqueous solvent[16]. This transformation significantly improves the binding affinity of cellulose to enzymes. Although cellulose III exhibits heightened sensitivity to specific chemical treatments, there are limited reports on the further functionalization of cellulose

aerogels or amine-treated fibers[17,18]. (Manuscript, page 3, lines 47-55)

Revision (2): … Building upon previously reported mature amine-treated cellulose processes[13,16,23–25], this study utilizes the competitive hydrogen bonds formed between small-molecule EDA and cellulose to disrupt the hydrogen bond network in pre-formed cellulose I aerogels, promoting molecular chain rearrangement and driving its crystalline isomerization towards the more reactive cellulose III. Our findings indicate that this process enhances the reactivity of cellulose III without compromising the macroscopic pore structure of the aerogel. Additionally, we developed a uniform polymer topological network through in-situ polymerization and crosslinking, achieving the objective of maintaining fiber stiffness while effectively shielding inter-fiber hydrogen bonds. Following topological isomerization, the cellulose I aerogel yielded a cellulose III-based triboelectric aerogel (CNF-III@Si) that exhibits both superelasticity and high strength. Moreover, this aerogel demonstrates an ultrafast compression recovery rate and temperature-invariant elasticity, thereby creating favorable conditions for applications in extreme environments. Topological isomerization, which induces electron cloud redistribution and alters microstructure, enhances triboelectric output performance. Consequently, triboelectric nanogenerators constructed from aerogels exhibit rapid response times and highly stable outputs. Moreover, the stable output signal, sustained across a broad range of temperatures and humidity levels, underscores its significant potential for high-precision flexible sensing in extreme environments. (Manuscript, page 4-5, lines 78-97)

Revision (3): … Traditional amine treatment of cellulose powder or film materials has been demonstrated to enhance cellulose reactivity[15,16,18,28]. Based on these findings, this study examines crystalline isomerization in the aerogel state to improve hydroxyl group accessibility and reorganize the hydrogen bond network, thereby increasing cellulose reactivity. By infiltrating anhydrous ethylenediamine (EDA) into the interior of the CNF-I aerogel fibers, the amino and hydroxyl groups formed strong competitive hydrogen bonds, disrupting the hydrogen bond network of cellulose[29]. (Manuscript, page 6, lines 110-114)

Revision (4): …The mature amine treatment process for cellulose facilitated the reconstruction of the hydrogen bond network, thereby enhancing the accessibility of hydroxyl groups in the cellulose aerogel while preserving the stiffness of the fibers. (Manuscript, page 28, lines 552-554)

DFT is performed on monomeric fragments of CNF-III@Si, which may not accurately capture the continuum Si–O–Si network. Authors should discuss limitations.

Response: We sincerely thank the reviewer for this rigorous comment, which helps improve the clarity and completeness of our study. We fully agree that the simplified DFT models based on monomeric or oligomeric CNF-III@Si fragments cannot fully capture the long-range order and collective electronic effects of the continuous Si–O–Si network in the real material. This simplification allows us to gain atomistic insight into local interactions and electronic property trends under limited computational resources.

To account for different local environments, we analyzed three CNF-III@Si models (Figure 5c–e):

Model 1: CNF-III chains without siloxane grafting (cellobiose tetramer representation);

Model 2: CNF-III chains partially grafted with siloxane (cellobiose tetramer grafted with one -$Si(OH)_2CH_3$, CNF-III@Si-1);

Model 3: Fully grafted cellulose chains forming a crosslinked topological network (cellobiose tetramer grafted at all C6 positions, CNF-III@Si-2).

We agree with the reviewer that these models cannot precisely represent the continuous Si–O–Si network and its long-range interactions. Therefore, the DFT calculations in this work are primarily qualitative, aimed at revealing trends in the electronic properties of cellulose fragments in different local chemical environments, particularly the effects of interfacial functional groups on charge distribution and charge transfer, rather than quantitatively describing the macroscopic electronic structure of the entire composite.

In the revised manuscript, we have explicitly discussed the limitations of these simplified models and clarified that the results are intended to illustrate local interactions and relative trends, not the quantitative behavior of the continuous siloxane network. We thank the reviewer again for their valuable suggestions, and the revised manuscript now clearly delineates the scope and theoretical boundaries of this work.

Revision (1): … Although these simplified models may diverge from reality, they are designed to elucidate the local electronic structure of the bonds between silanes and the cellulose surface, as well as the fundamental trends in charge transfer. This approach provides valuable insights into the potential distribution, charge generation, and transfer

of CNF-III@Si. The electrostatic potential distribution indicates that CNF-III, CNF-III@Si-1, and CNF-III@Si-2 all exhibit favorable electropositive properties (Fig. 5d), rendering them suitable candidates for triboelectric materials. (Manuscript, page 25-26, lines 485-492)

Revision (2): … It is important to note that these models may not accurately represent real reactivity or actual charge transfer processes. However, they offer valuable insights into the changes in reactivity at the molecular level and elucidate how electrons are generated and transferred in aerogels during contact separation. (Manuscript, page 36, lines 696-699)

Revision (3): … For the CNF-III@Si system, we constructed three representative models to facilitate a comprehensive analysis that aligns more closely with the material's potential structures, rather than relying on a single model. The first model features an ungrafted CNF-III chain, represented by a single fiber tetrasaccharide unit. In the second model, a -$Si(OH)_2CH_3$ group is grafted onto the fiber tetrasaccharide skeleton, denoted as CNF-III@Si-1. The third model, referred to as CNF-III@Si-2, involves siloxane grafting at all C6 sites of the tetrasaccharide unit to simulate a cross-linked polymer network structure. The simplification of these models reflects a balance between computational resource limitations and the necessity for atomic-level analysis of core interactions. Additionally, for regular polymers such as fluorinated ethylene propylene (FEP), this study employs their periodic repeating units as the computational model, a widely accepted approach in DFT calculations for examining the electronic

structure of polymers. (Supplementary Information, page 5-7)

Reviewer #5 (Remarks to the Author):

I co-reviewed this manuscript with one of the reviewers who provided the listed reports. This is part of the Nature Communications initiative to facilitate training in peer review and to provide appropriate recognition for Early Career Researchers who co-review manuscripts.

Response: we sincerely thank the co-reviewer for the time, care, and thoughtful insights contributed through the Nature Communications co-review initiative. The detailed and rigorous comments—particularly those highlighting points that might otherwise have been overlooked—have been extremely valuable in improving the clarity, rigor, and overall quality of the manuscript. We greatly appreciate this careful and professional review.

Point-by-Point Response to Reviewers' Comments

Response summary: We extend our heartfelt gratitude to the editor and reviewers for the insightful feedback on our manuscript titled "*Topological Isomerization Unlocks Exceptional Elasticity and Strength of Cellulosic Triboelectric Aerogels*" (Manuscript ID: NCOMMS-25-87076A), which greatly improved our manuscript.

Reviewer #2 (Remarks to the Author):

The current manuscript has perfectly addressed my questions and is ready for publication in Nature Communications.

Response: We sincerely thank the reviewer for the positive and encouraging evaluation of our revised manuscript. We greatly appreciate your careful assessment and recognition that the manuscript has satisfactorily addressed your concerns. Your constructive comments have been invaluable in improving the quality and clarity of our work.

Reviewer #3 (Remarks to the Author):

In this revised paper, authors revised the paper according to the comments. Therefore, it can be accepted now.

Response: We sincerely thank the reviewer for the careful re-evaluation of our manuscript. We greatly appreciate your recognition of the revisions made in response to the comments and your support for the acceptance of our work. Your constructive feedback has been instrumental in improving the quality of the manuscript.

Reviewer #4 (Remarks to the Author)

I thank the authors for the thorough, careful, and technically detailed revision of the manuscript. The revised version addresses all major and minor comments raised in the initial review in a comprehensive and convincing manner. The authors have significantly improved the clarity and rigor of the manuscript.

Response: We sincerely thank the reviewer for the thorough re-evaluation of our manuscript and for the generous and encouraging comments. Your insightful and constructive feedback has been invaluable in strengthening the manuscript.

One minor point remains regarding the manuscript structure. In the initial review, I suggested strengthening the Discussion section. While the authors have added a clarifying sentence, the standalone Discussion remains relatively short, whereas the Results section is very extensive and already contains a substantial amount of interpretation and contextual discussion. To better reflect the actual content and improve readability, I recommend renaming the Results section to “Results and Discussion”, and renaming the current Discussion section to “Conclusion” if the journal allows this. This is an editorial adjustment and does not require additional experimental or analytical work.

Response: We sincerely thank the reviewer for this suggestion. We fully understand and appreciate the recommendation to rename the “Results” section as “Results and Discussion” and to retitle the current “Discussion” section as “Conclusion” to better reflect the content organization and improve readability. However, according to the

formatting guidelines of *Nature Communications*, the main text should not contain a standalone "Conclusion" section. To ensure full compliance with the journal's structural requirements, we have therefore retained the original section titles. We are nonetheless very grateful for this editorial suggestion.

Overall, the manuscript has been significantly strengthened and now meets the standards of scientific clarity, methodological rigor, and internal consistency expected for publication. I recommend acceptance of the manuscript.

Response: We sincerely thank the reviewer for the positive evaluation and recommendation for acceptance. We greatly appreciate your recognition of the improved clarity and rigor of the manuscript.

Reviewer #5 (Remarks to the Author):

I co-reviewed this manuscript with one of the reviewers who provided the listed reports. This is part of the Nature Communications initiative to facilitate training in peer review and to provide appropriate recognition for Early Career Researchers who co-review manuscripts.

Response: We sincerely thank the reviewer for the positive and encouraging evaluation of our revised manuscript. We greatly appreciate your careful assessment and recognition that the manuscript has satisfactorily addressed your concerns. Your constructive comments have been invaluable in improving the quality and clarity of our work.